Biointerface Research in Applied Chemistry
Platinum Open Access Journal (ISSN: 2069-5837)

Article
Volume 10, Issue 6, 2020, 6783 - 6809
https://doi.org/10.33263/BRIAC106.67836809

Vibrational Studies of Species Derived from Potent S(+) and R(-) Ecstasy Stimulant by Using *Ab-initio* Calculations and the SQM Approach

Karina A. Guzzetti [1], Maximiliano A. Iramain [1], Roxana A. Rudyk [1], Maria E. Manzur [1], Silvia Antonia Brandán [1,*]

[1] Cátedra de Química General, Instituto de Química Inorgánica, Facultad de Bioquímica. Química y Farmacia, Universidad Nacional de Tucumán, Ayacucho 471, (4000) San Miguel de Tucumán, Tucumán, Argentina
* Correspondence: sbrandan@fbqf.unt.edu.ar;

Scopus Author ID 6602262428
Received: 24.04.2020; Revised: 24.05.2020; Accepted: 25.05.2020; Published: 27.05.2020

Abstract: B3LYP/6-311++G** calculations and the scaled quantum mechanical force field (SQMFF) approach have been used to study the structures and vibrational spectra of three species derived from potent S(+) and R(-) ecstasy stimulant. The complete vibrational assignments of free base, cationic, and hydrochloride species of both enantiomeric forms of ecstasy have been reported by using the normal internal coordinates and the experimental available attenuated total reflectance ATR-IR and FT-Raman spectra. SQM calculations predicted that the three species could be present in the IR spectrum of hydrochloride species because the IR bands of medium intensity at 2794 cm^{-1} is assigned to the stretching C4-H15 and symmetric CH_3 modes of the free base while the strong IR band at 1508 cm^{-1} is assigned easily to NH_2 stretching mode of hydrochloride species and NH_2 deformation modes of cationic species. The calculations reveal the same energy values for both enantiomers, indicating that both could exist simultaneously in the two media with similar corrected solvation energies in solution probably because the R(-) form is quickly converted to the S(+) one. Three types of charges studied in both media evidence higher effect on the N atoms belonging to N-CH_3 groups of three species of S(+) form of ecstasy in both media than on the O atoms of R1 ring. The high gap value predicted for the hydrochloride species of S(+) form in solution supports the low reactivity of this species, in agreement to its higher stability evidenced in this medium by AIM and NBO calculations. The predicted Ultraviolet-visible and Electronic Circular Dichroism ecstasy (ECD) support the presence of both enantiomeric forms in solution while excellent concordance evidence the comparisons between the predicted ^{1}H- and ^{13}C-NMR chemical shifts for the three species of S(+) form of ecstasy with the corresponding experimental ones.

Keywords: Ecstasy; Force fields; Vibrational analysis; DFT calculations; Molecular structure.

1. Introduction

For several years our research group has been interested in the study of different species containing the N-CH_3 group and, in particular, tropane alkaloids because they present different biological activities and multiple effects [1-7] while other compounds containing the same group show antihistaminic, anti-hypertensive and psychotropic effects [8-14]. *Ab-Initio* studies on some alkaloids have revealed essential changes in the charges, in electronic densities of rings and stabilization, and solvation energies when the N-CH_3 group is linked to fused rings. At the same time, the N-C distance between the two atoms of that group plays an essential role

in the stability of species [7]. On the other hand, vibrational studies of hydrochloride/hydrobromide forms of scopolamine, morphine, heroin, cocaine, tropane, diphenhydramine, cyclizine, 2-CB, gramine, guanfacine, promethazine, naloxone, tolazoline, and clonidine combining DFT calculations with the SQMFF methodology have demonstrated that the cationic forms of these species are present in the solid phase and aqueous solution [1-3,5-18]. This way, the strong IR bands predicted between 2700 and 1500 cm^{-1}, and assigned to the N-H stretching modes in hydrochloride/hydrobromide species by using B3LYP/6-31G* calculations, are not present in the corresponding experimental spectra [1-3,5-18]. Then, the presence of Cl atom in the hydrochloride species shifts the N-H stretching modes toward lower wavenumbers, as compared with the observed for the cationic species (3350 and 3150 cm^{-1}) [19]. Hence, those previous studies have shown that hydrochloride drugs should also be studied in their free base and cationic forms and, specifically, in aqueous solution. As a continuation of studies related to species containing N-CH_3 groups of great medicinal and/or pharmacological interest, in this work, the structural, electronic, topological, and vibrational properties of three forms of powerful ecstasy stimulant were evaluated [20-23]. The generic and chemical names of ecstasy hydrochloride are respectively ecstasy and 3,4-Methylenedioxymethamphetamine (MDMA), while its IUPAC name is 1-(1,3-benzodioxol-5-yl)-N-(trideuteriomethyl)propane-2-amine hydrochloride. Then, its Molecular Formula is $C_{11}H_{16}ClNO_2$. Structurally, ecstasy has a chiral center, and, for this reason, two S(+) and R(-) enantiomers are expected for its free base, cationic, and hydrochloride species. The experimental structure of S(+) ecstasy hydrochloride was determined by X-ray diffraction by Morimoto et al. [23] but, so far, the structural properties and complete vibrational assignments of those three species of ecstasy were not published. Here, it is essential to mention that the use of MDMA is internationally controlled because this synthetic drug acts as a central nervous system stimulant and has a weak hallucinogenic property for which is broadly used to psychiatric therapy and, for these reasons, its use is minimal [20-22]. Therefore, for a long time, the first techniques used to control and identify that illicit drug in many preparations were mass, NMR, and vibrational spectroscopies together with the gas chromatography [20,22,24-43]. Usually, the gas chromatography is used for impurity ecstasy samples, while the NMR and vibrational spectroscopy are techniques employed to identification and quantification of pure substances [20-22,24-31,33-37,39-42]. In this work, the theoretical S(+) and R(-) structures of those three ecstasy species were optimized in the gas phase and aqueous solution by using the hybrid B3LYP/6-311++G** level of theory [44,45]. The studies in solution were performed with the integral equation formalism variant polarised continuum method (IEFPCM) because its technique contemplates the solvent effects. At the same time, the uncorrected and corrected solvation energies by zero-point vibrational energy (ZPVE) and non-electrostatic terms were computed with the universal solvation model [46-48]. For those three ecstasy species, atomic charges, molecular electrostatic potential, bond orders, frontier orbitals, and topological properties were calculated together with the harmonic force fields by using the scaled mechanical force field (SQMFF) and transferable scaling factors [49,50]. Then, the complete assignments for the three species were performed by using the corresponding force fields, normal internal coordinates, the Molvib program [51], and the experimental available infrared spectrum of the free base and hydrochloride ecstasy [20-22,26,52]. Taking into account that experimental study, the S(+) form is most active than R(-) one [53,54]. However, the latter form is bio-transformed faster than the S(+) one [53], the reactivities and behaviors for the three species of both enantiomeric forms were predicted in both media by using the frontier

orbitals [55,56] and global descriptors [57-65]. Later, comparisons among the three species of both enantiomeric forms were performed.

2. Materials and Methods

The initial S(+) ecstasy hydrochloride structure was that experimental taken from the available CIF file determined by X-ray diffraction by Morimoto et al. [23]. The corresponding cationic and free base species were modeled, removing first the Cl atom from that initial structure of ecstasy hydrochloride and at continuation, the H atom respectively by using the *GaussView* program [66]. This program was also used to model the R(-) structures of ecstasy considering those reported structures by Zapata-Torres et al. and Lourenço et al. [31,43]. The optimizations of all species of both enantiomers in both media were carried out with the Revision A.02 of the Gaussian program [67] and the hybrid B3LYP/6-311++G** method [44,45]. The structural differences between the free bases of both enantiomers can be seen in **Figure 1** through planar and tri-dimensional structures.

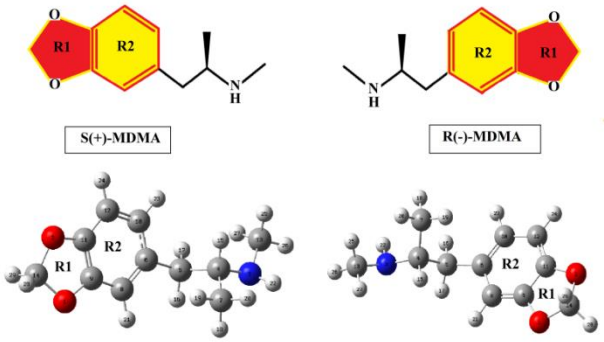

Figure 1. Molecular structures of free bases of S(+) and R(-) of ecstasy with the identifications of both rings and atoms numbering.

All species were optimized in solution by using PCM and SMD calculations [46-48] while the volume changes were computed with the Moldraw program [68]. The three S(+) species of ecstasy and the identifications of the two rings are given in **Figure 2,** while the corresponding to R(-) ones can be seen in **Figure 3** together with the atoms labeling.

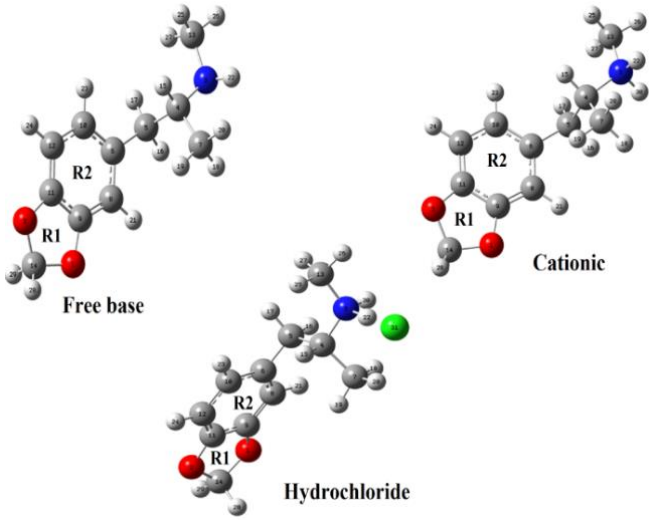

Figure 2. Molecular structures of the free base, cationic, and hydrochloride species of S(+) ecstasy with the identifications of both rings and atoms numbering.

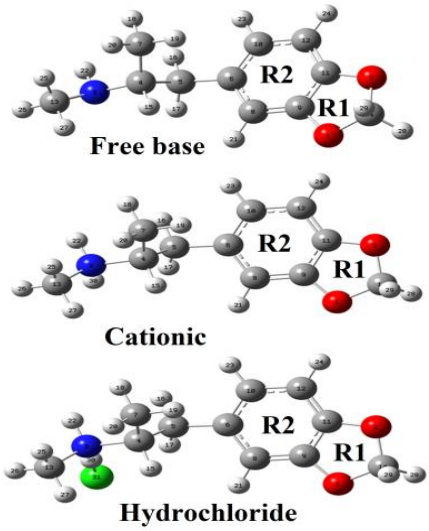

Figure 3. Molecular structures of the free base, cationic, and hydrochloride species of R(-) ecstasy with the identifications of both rings and atoms numbering.

For all species, natural population atomic (NPA) charges, molecular electrostatic potentials, bond orders, main delocalization energies, and topological properties were calculated with the versions 5.1 and 2000 of NBO and AIM programs, respectively [69,70] while the frontier orbitals were used to calculate the gap values defined as the difference between both orbitals [55,56]. Then, the chemical potential (μ), electronegativity (χ), global hardness (η), global softness (S), global electrophilicity index (ω) and global nucleophilicity index (E) descriptors were computed using reported equations [57-65]. Harmonic force fields of all species in both media were computed with the SQMFF approach and the Molvib program [49-51]. The vibrational assignments of all bands observed in the experimental available infrared and Raman spectra for the free base and ecstasy hydrochloride in the solid phase [21,22,26,52] were performed by using the normal internal coordinates and Potential Energy Distribution (PED) contributions ≥ 10%. To a better correlation, the predicted Raman spectra in activities were corrected to intensities [71,72]. The GIAO method [73] was employed to predict ^{1}H- and ^{13}C-NMR chemical shifts, which were compared with the corresponding experimental ones available from the literature [21,22,27,31,37,40,41]. Finally, Time-dependent DFT calculations (TD-DFT) calculations were performed to predict the ultraviolet-visible and electronic circular dichroism spectra of all species in water using the same level of theory and the Gaussian 09 program [67].

3. Results and Discussion

3.1. Structural study in both media.

In Table 1 are summarized the calculated total uncorrected and corrected by zero-point vibrational electronic (ZPVE) energies, dipole moments, and volumes for the three species of both enantiomers of ecstasy as a free base, cationic and hydrochloride forms in gas and aqueous solution phases by using the B3LYP/6-311++G** method. The results of Table 1 show that the three species have practically the same energy values in both enantiomers. However, some variations in μ values are observed among them. Hence, the two enantiomers can exist simultaneously in the two media. Note that the corrected values by ZPVE are smaller than the uncorrected because the vibrations even persist in zero Kelvin. Besides, in both media, the

cationic forms of S(+) and R(-) present high μ values but higher values in solution because these species are charged in this medium and hydrated with water molecules. Calculated volumes for all species of ecstasy in the gas phase and its variations in solution are presented in Table 2.

Slight increase of V in aqueous solution is observed in all species of S(+) and R(-) forms with the exception of cationic species of R(-) form, which shows a volume contraction instead V expansion in this medium. Table 3 is given the uncorrected and corrected solvation energies only due to total non-electrostatic terms, while in Table 4 are also presented the solvation energies, including corrections by ZPVE (ΔGc/ZPVE).

Table 1. Calculated total energy (*E*) and dipolar moments for the three species of both enantiomers of ecstasy at the B3LYP/6-311++G** level of theory.

B3LYP/6-311++G** method						
S(+)-MDMA	Gas-phase			Aqueous solution		
	Freebase	Cationic	Hydrochloride	Freebase	Cationic	Hydrochloride
E (Hartrees)	-633.549	-633.926	-1094.404	-633.561	-634.029	-1094.446
$E^{\#}$ (Hartrees)	-633.303	-633.666	-1094.146	-633.315	-633.768	-1094.185
μ (Debye)	0.67	14.43	8.75	1.24	18.62	13.38
R(-)-MDMA	Freebase	Cationic	Hydrochloride	Freebase	Cationic	Hydrochloride
E (Hartrees)	-633.548	-633.927	-1094.126	-633.560	-634.030	-1094.146
E# (Hartrees)	-633.303	-633.667	-1094.148	-633.314	-633.769	-1094.186
μ (Debye)	1.32	14.24	8.61	2.43	18.43	13.66

[#]Value corrected by ZPVE

Table 2. Calculated Molar Volume (Å^3) for the three species of ecstasy in the gas phase and aqueous solution by using the B3LYP/6-311G** level of theory.

B3LYP/6-311++G** method			
Species	Gas-phase	Aqueous solution	ΔV(Vsol -Vgas)
S(+)-MDMA			
Free Base	216.6	219.2	2.6
Cationic	219.1	220.0	0.9
Hydrochloride	243.7	248.0	4.3
R(-)-MDMA			
Free Base	219.6	222.0	2.4
Cationic	223.8	223.2	-0.6
Hydrochloride	247.6	250.0	2.4

Table 3. Corrected and uncorrected solvation energies by the total non-electrostatic terms for the three species of ecstasy in the gas phase and aqueous solution by using the B3LYP/6-311++G** level of theory.

R(-)-MDMA			
Solvation energy (kJ/mol)			
Species	ΔG_u	ΔG_{ne}	ΔG_c
Free base	-31.47	14.67	-46.14
Cationic	-270.17	27.38	-297.55
Hydrochloride	-52.46	26.75	-79.21
S(+)-MDMA			
Species	ΔG_u	ΔG_{ne}	ΔG_c
Free base	-31.47	14.00	-45.47
Cationic	-270.17	27.21	-297.38
Hydrochloride	-110.17	26.67	-136.84

ΔG_u= uncorrected solvation energy, ΔG_{ne}= total nonelectrostatic terms, ΔG_c= corrected solvation energies.

The results observed in Table 3 show that the corrected solvation energies only by complete non-electrostatic terms of cationic species of both forms are practically the same in solution probably because the R(-) form is quickly converted to the S(+) one while both free base and hydrochloride forms of two enantiomers have values slightly different in this medium. When the corrected and uncorrected solvation energies by the total non-electrostatic terms and

by ZPVE values are analyzed with detail from Table 4 it is newly observed that the cationic species of both enantiomers evidence the same values although slightly lower than those uncorrected by ZPVE, possibly due to the transformation of R(-) form to S(+), as was above mentioned [53].

Table 4. Corrected and uncorrected solvation energies by the total non-electrostatic terms and by ZPVE for the three species of ecstasy in the gas phase and aqueous solution by using the B3LYP/6-311G** level of theory.

R(-)-MDMA			
Solvation energy (kJ/mol)			
Species	ΔG_u	ΔG_{ne}	$\Delta G_{c/ZPVE}$
Free base	-28.85	14.67	-43.52
Cationic	-267.54	27.38	-294.92
Hydrochloride	-99.67	26.75	-126.42
S(+)-MDMA			
	ΔG_u	ΔG_{ne}	$\Delta G_{c/ZPVE}$
Free base	-31.47	14.00	-45.47
Cationic	-267.54	27.21	-294.75
Hydrochloride	-102.30	26.67	-128.97

ΔG_u= uncorrected solvation energy by ZPVE, ΔG_{ne}= total nonelectrostatic terms, ΔG_c= corrected solvation energies.

Table 5. Corrected solvation energies by the total non-electrostatic terms and by ZPVE ($\Delta G_{c/ZPVE}$) for the three ecstasy species compared with reported values for other alkaloids.

B3LYP/6-311++G**			B3LYP/6-31G*				
Ecstasy			Scopolamine[b]	Heroin[c]	Morphine[d]	Cocaine[e]	2-CB[f]
Species	S(+)	R(-)					
Free base	-45.47	-43.52	-75.47	-88.67	-60.91	-71.26	-49.31
Cationic	-294.75	-294.92	-310.34	-323.14	-309.19	-255.24	-308.69
HCl/HBr[#]	-128.97	-126.42	-122.74	-161.94	-144.74	-138.14	-122.58

[a]This work, [f]rom Ref [1], [f]rom Ref [3], [f]rom Ref [5], [e]From Ref [7], [f]rom Ref [10]

Table 5 shows comparisons among corrected solvation energies ($\Delta G_{c/ZPVE}$) for the three ecstasy species with those reported for scopolamine, heroin, morphine, cocaine, and 2-CB (4-Bromo-2,5-dimethoxyphenethylamine) alkaloids [1,3,5,7,10]. The graphics of $\Delta G_{c/ZPVE}$ for the three species of ecstasy are compared with the corresponding to those alkaloids in Figure 4. Proximities between 6 and -4 kJ/mol can be easily seen in Fig. 4 for the $\Delta G_{c/ZPVE}$ values of free base and hydrochloride species of both forms of ecstasy with the values corresponding to psychotropic agent 2-CB and to scopolamine, respectively. However, the higher variations are observed for the cationic species of ecstasy with the value corresponding to 2-CB, whose observed differences are between -13.94 and -13.77 kJ/mol. These results are in agreement with the biological properties evidenced in these three alkaloid species.

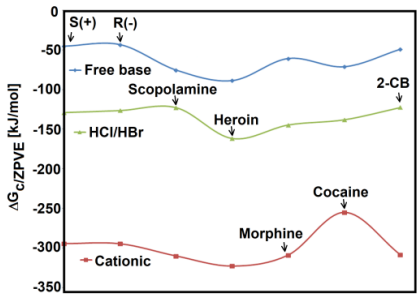

Figure 4. Corrected solvation energies by the total non-electrostatic terms and by ZPVE for the three ecstasy species compared with reported values for other alkaloids. 2-CB: 4-Bromo-2,5-dimethoxyphenethylamine.

The high $\Delta G_{c/ZPVE}$ values (most negative values) observed in the cationic forms of all compared alkaloids are due to that the hydrochloride species or, hydrobromide in the scopolamine case, are present in aqueous solution and they are charged species with high dipole

moment values and, as a consequence, are hydrated in solution. The differences observed between the $\Delta G_{c/ZPVE}$ values of three species of ecstasy with the corresponding to 2-CB or scopolamine could be attributed to the calculations because here the solvation energies values are predicted by using the B3LYP/6-311++G** method while in the other alkaloids were calculated with the B3LYP/6-31G* level of theory.

3.2. Geometrical parameters in both media.

The optimizations for the three species of both S(+) and R(-) forms of ecstasy have predicted similar energies values among them, as observed in Table 1, and for another side, taking into account that the R(-) form is transformed to the S(+) one here only the calculated geometrical parameters for the three S(+) ecstasy species in both media by using the B3LYP/6-311++G** method are presented in Table 6 compared with the corresponding experimental ones, determined by Morimoto et al. [23] for the hydrochloride form. The root means square deviation (RMSD) values are used to compare the differences between experimental and theoretical ones. Better correlations are observed for the hydrochloride species in both media, as expected because its form is experimentally compared. Thus, the RMSD values for bond lengths and angles in all species are between 1.016-0.008 Å and 1.3-0.9 º, respectively. On the other side, the dihedral N3-C4-C5-C6 and C7-C4-C5-C6 angles show good concordances in the three species, as compared with the corresponding experimental ones and, where in general the RMSD values of hydrochloride species present reasonable correlations in both media (90.8 º). Both rings methylenedioxy and phenyl rings are basically coplanar, while the orientation of the isopropylamine group with the C7 atom (C7-C4-C5-C6) predicted dihedral angles similar to that experimentally reported of 66.4 º [23]. The exhaustive observation of all bond lengths shows that the N3-C4 and N3-C13 distances for the free base in both media are predicted with lower values than the cationic and hydrochloride ones in both media. On the other hand, the calculated bonds N-CH_3 lengths of three ecstasy species compared with the corresponding to the reported for scopolamine, heroin, morphine, cocaine, tropane, and 2-CB alkaloids species in gas and aqueous solution phases by using B3LYP/6-31G* level of theory are presented in Table 7 [1-7]. In Figure 5 are graphed the variations in the N-CH_3 distances for the three species of S(+) forms of ecstasy in both media with those other compared species by using different levels of theory. Hence, different behaviors are observed for those three species in the gas phase, as compared with the corresponding predicted in aqueous solution.

Table 6. Calculated geometrical parameters for the three S(+) ecstasy species in both media by using the level B3LYP/6-311++G** compared with the corresponding experimental ones for the ecstasy hydrochloride.

Parameter	Gas-Phase			Aqueous solution			Exp.[b]
	Freebase	Cationic	HCl	Freebase	Cationic	HCl	
Bond lengths (Å)							
O1-C9	1.377	1.363	1.373	1.388	1.386	1.387	1.373
O1-C14	1.433	1.441	1.434	1.440	1.441	1.440	1.429
O2-C11	1.378	1.363	1.374	1.388	1.386	1.387	1.385
O2-C14	1.432	1.438	1.433	1.439	1.440	1.440	1.430
N3-C4	1.468	1.547	1.503	1.478	1.524	1.516	1.497
N3-C13	1.460	1.503	1.483	1.468	1.495	1.491	1.490
C4-C5	1.549	1.538	1.543	1.546	1.538	1.539	1.535
C4-C7	1.528	1.523	1.527	1.526	1.523	1.524	1.517
C5-C6	1.514	1.517	1.516	1.514	1.515	1.515	1.507
C6-C8	1.410	1.411	1.409	1.411	1.410	1.410	1.402
C6-C10	1.399	1.396	1.398	1.400	1.398	1.399	1.392
C8-C9	1.378	1.378	1.378	1.379	1.378	1.410	1.373
C9-C11	1.389	1.394	1.390	1.387	1.388	1.388	1.384
C10-C12	1.404	1.404	1.404	1.405	1.405	1.405	1.408
C11-C12	1.378	1.378	1.378	1.378	1.378	1.378	1.363
RMSD[b]	0.013	0.016	0.008	0.011	0.010	0.013	

Parameter	Gas-Phase			Aqueous solution			Exp.[b]
	Freebase	Cationic	HCl	Freebase	Cationic	HCl	
Bond lengths (Å)							
Bond angles (º)							
C9-O1-C14	104.8	105.8	105.0	104.7	104.8	104.6	105.8
C11-O2-C14	104.7	106.0	105.0	104.6	104.8	104.5	105.6
C4-N3-C13	115.4	116.8	117.5	113.3	116.7	116.4	115.3
N3-C4-C5	109.6	109.4	111.8	110.2	109.1	110.5	110.3
N3-C4-C7	109.1	107.5	107.9	109.3	107.7	107.9	107.9
C5-C4-C7	111.8	114.6	113.6	112.1	114.2	113.5	113.3
C4-C5-C6	114.4	112.1	113.3	114.1	113.0	112.6	111.1
C5-C6-C8	120.3	119.9	120.2	120.4	119.8	120.2	117.9
C5-C6-C10	120.4	119.9	120.1	120.2	120.3	120.0	121.8
C8-C6-C10	119.3	120.2	119.7	119.4	119.8	119.8	120.3
C6-C8-C9	117.8	117.4	117.6	117.6	117.4	117.4	117.2
O1-C9-C8	128.4	128.3	128.4	128.3	128.3	128.4	127.9
O1-C9-C11	109.4	109.8	109.5	109.4	109.4	109.3	110.2
C8-C9-C11	122.1	122.0	122.1	122.3	122.2	122.2	121.9
C6-C10-C12	122.4	121.8	122.1	122.4	122.1	122.2	121.9
O2-C11-C9	109.5	109.6	109.5	109.5	109.5	109.4	109.5
O2-C11-C12	129.0	128.7	128.9	128.9	128.8	128.8	128.0
C9-C11-C12	121.5	121.7	121.6	121.6	121.7	121.7	122.5
C10-C12-C11	116.9	116.9	116.9	116.7	116.8	116.7	116.3
O1-C14-O2	107.3	107.0	107.2	106.7	106.7	106.6	108.5
N3-H22-Cl31			174.8			171.0	173.3
RMSD[b]	1.2	0.9	1.1	1.3	1.0	1.0	
Dihedral angles (º)							
C14-O1-C9-C8	-169.8	-172.9	170.7	-168.7	-169.3	168.4	177.2
C14-O1-C9-C11	12.2	8.3	-11.7	13.7	13.1	-14.2	-3.5
C9-O1-C14-O2	-19.8	-13.3	18.8	-22.1	-21.0	22.8	5.9
C14-O2-C11-C9	-12.4	-8.5	11.8	-13.9	-13.2	14.2	3.9
C14-O2-C11-C12	169.6	172.6	-171.0	168.3	169.2	-168.6	-177.0
C11-O2-C14-O1	19.9	13.4	-18.8	22.2	21.1	-22.8	-6.0
C13-N3-C4-C5	-98.5	72.7	57.9	79.1	72.1	59.4	65.9
C13-N3-C4-C7	-159.4	-162.3	-176.5	-157.2	72.1	-175.9	-170.0
N3-C4-C5-C6	-172.1	-173.5	-174.4	-167.3	-176.9	-173.2	-172.5
C7-C4-C5-C6	66.7	65.7	63.2	70.7	62.6	65.5	66.4
C4-C5-C6-C8	-102.9	-100.8	-102.8	-99.5	-100.1	-102.3	108.2
C10-C6-C8-C9	0.0	-0.2	-0.5	0.0	0.1	-0.5	-0.3
C5-C6-C10-C12	-179.4	-179.3	-179.1	-179.3	-179.7	-179.2	178.2
C6-C8-C9-O1	-178.0	-178.8	177.6	-177.7	-177.5	177.4	178.7
O1-C9-C11-C12	178.3	179.1	-177.6	178.1	177.9	-177.4	-179.3
C8-C9-C11-O2	-178.0	-178.7	177.8	-177.7	-177.7	177.6	179.0
C8-C9-C11-C12	0.1	0.3	0.3	0.3	0.1	0.2	-0.0
C6-C10-C12-C11	-0.3	-0.3	0.1	-0.2	-0.3	0.2	-0.1
O2-C11-C12-C10	177.9	178.8	-177.4	177.5	177.5	-177.3	-178.5
C4-N3-H22-Cl31	-	-	-107.0	-	-	-129.1	-121.4
C13-N3-H22-Cl31	-	-	19.1	-	-	-2.7	0.5
RMSD[b]	223.8	221.2	90.9	220.2	227,2	90.8	

[a]This work, [f]rom Ref [23]

Table 7. Calculated bond N-CH_3 lengths of three species of S(+) form of ecstasy compared with the corresponding to some alkaloids species in the gas phase and aqueous solution by using different levels of theory.

Species	B3LYP/6-311++G** method[a]					
	GAS PHASE			AQUEOUS SOLUTION		
	Freebase	Cationic	Hydrochloride	Freebase	Cationic	Hydrochloride
Ecstasy[a]	1.460	1.503	1.483	1.468	1.495	1.491
B3LYP/6-31G* method						
Scopolamine[b,#]	1.462	1.492	1.491	1.466	1.491	1.493
Heroin[c]	1.453	1.501	1.483	1.460	1.498	1.492
Morphine[d]	1.453	1.500	1.483	1.460	1.497	1.493
Cocaine[e]	1.459	1.493	1.487	1.467	1.492	1.494
Tropane[f]	1.458	1.496	1.478	1.467	1.491	1.486
2-CB[g]	1.463	1.535	1.476	1.468	1.505	1.497

[#]Hydrobromide, [a]This work, [b]from ref [7], [c]from ref [5], [d]from ref [1], [e]from ref [3], [f]from ref [2], [g]from ref [10], 2-CB: 4-Bromo-2,5-dimethoxyphenethylamine.

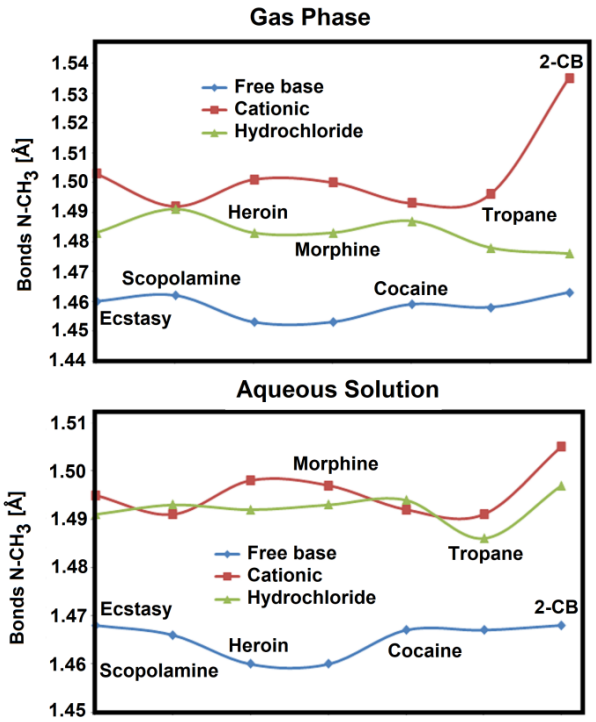

Figure 5. Calculated bonds N-CH_3 lengths of three species of S(+) form of ecstasy compared with the corresponding to some alkaloids species in the gas phase (upper) and aqueous solution (bottom) by using different levels of theory. 2-CB: 4-Bromo-2,5-dimethoxyphenethylamine.

Here, it is essential to mention that all free base species in solution have practically the same behaviors than those observed in the gas phase, increasing the values slightly in solution, as detailed in Table 7. First, the free base species of S(+) forms of ecstasy in both media (blue line) present the lowest distances having the species of scopolamine and cocaine the higher values in the gas phase. In comparison, heroin and morphine in both media show lower values. However, higher distances are observed when all cationic (red line) and hydrochloride species (green line) are compared, presenting the two species of 2-CB the highest values in solution. In contrast, their cationic form in the gas phase shows a surprisingly high value. Such observations are justified because the N-C distances in the three species of 2-CB correspond to primary amines, as shown by red circles in Figure 6; in the species of ecstasy correspond to secondary amines (blue circles in Fig. 6) while in the other alkaloids correspond to tertiary amines.

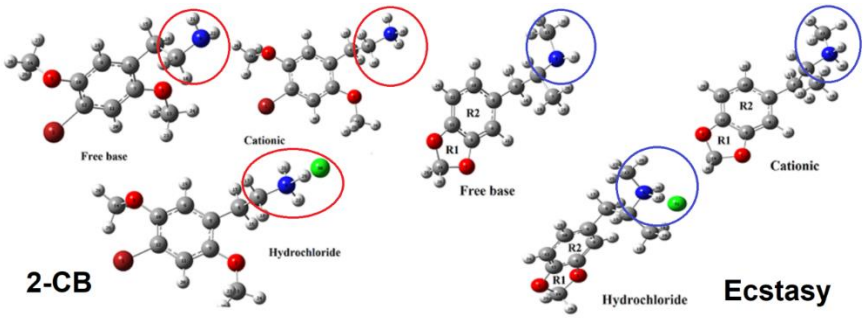

Figure 6. Molecular structures of three free base, cationic, and hydrochloride species of ecstasy and 2-CB (4-Bromo-2,5-dimethoxyphenethylamine) showing in the red circle the primary amines and with blue circles the secondary ones.

Obviously, in the gas phase, a species has greater freedom of movement and, particularly, when the N atoms are linked to lighter atoms like (H) in a primary amine, as are the cases of three species of 2-CB. On the other hand, the hydrochloride/hydrobromide and

cationic species show cross behaviors and closer in the solution where the higher values are observed in the cationic species and hydrochloride species of 2-CB, and the smallest value presents the hydrochloride species of tropane. Previous, structural, and vibrational studies have shown that the hydrobromide or hydrochloride species of some alkaloids are in solution as cationic ones [1-5,7,10,12,14]. These studies clearly show the influence of medium on the N-CH_3 distances independently of diverse groups linked to N atom. Besides, Lazni et al. have suggested by using combined DFT calculations and NMR studies the fast inversion of N-CH_3 group in solution [74].

3.3. Natural population atomic (NPA) charges, bond orders (BO), and molecular electrostatic potentials (MEP) studies.

Rudyk et al. [6,7] have suggested that the charges on the N and C atoms belonging to N-CH_3 groups in some tropane alkaloids could, in part, be indicative parameters to predict the potency of these alkaloids because those groups are commons to all alkaloids. Hence, taking into account that the S(+) ecstasy species are secondary amines and have N-CH_3 groups, the natural population atomic (NPA) and Mulliken charges, bond orders and molecular electrostatic potentials were studied for the three species by using the NBO 3.1 program [69] and Merz-Kollman (MK) charges [75]. Hence, calculated atomic MK, Mulliken, and natural population (NPA) charge on the essential atoms of three ecstasy species in gas and aqueous solution phases by using B3LYP/6-311++G** level of theory can be seen in Table 8. Behaviors of three atomic charges on the O, N, H, and Cl atoms of three S(+) ecstasy species in both media can be seen in Figure 7.

Table 8. MK, Mulliken, and Natural population atomic (NPA) charges observed on atoms of the three S(+) ecstasy species in gas and aqueous solution phases by using B3LYP/6-311++G** levels of theory.

S(+)-MDMA Gas Phase									
	Freebase			Cationic			Hydrochloride		
Atoms	MK	Mulliken	NPA	MK	Mulliken	NPA	MK	Mulliken	NPA
1 O	-0.442	-0.152	-0.544	-0.397	-0.134	-0.528	-0.436	-0.148	-0.539
2 O	-0.444	-0.155	-0.545	-0.396	-0.127	-0.524	-0.414	-0.144	-0.539
3 N	-0.811	-0.006	-0.679	-0.176	-0.044	-0.541	0.070	-0.017	-0.630
4 C	0.504	-0.684	-0.006	0.127	-0.643	0.012	0.131	-0.612	0.004
13 C	-0.002	-0.306	-0.359	-0.230	-0.276	-0.359	-0.372	-0.320	-0.362
22 H	0.381	0.215	0.344	0.301	0.317	0.424	0.014	0.082	0.389
30 H				0.294	0.342	0.421	0.251	0.324	0.384
31 Cl							-0.607	-0.460	-0.696
S(+)-MDMA Aqueous Solution									
Atoms	MK	Mulliken	NPA	MK	Mulliken	NPA	MK	Mulliken	NPA
1 O	-0.497	-0.220	-0.571	-0.475	-0.217	-0.568	-0.496	-0.218	-0.569
2 O	-0.476	-0.223	-0.572	-0.484	-0.217	-0.569	-0.479	-0.216	-0.570
3 N	-0.985	-0.174	-0.708	-0.127	0.080	-0.539	0.027	0.252	-0.595
4 C	0.630	-0.556	-0.009	0.372	-0.647	0.012	0.339	-0.677	0.011
13 C	0.086	-0.352	-0.372	-0.311	-0.351	-0.358	-0.296	-0.396	-0.364
22 H	0.443	0.261	0.362	0.334	0.351	0.449	0.209	0.103	0.458
30 H				0.312	0.372	0.446	0.277	0.378	0.433
31 Cl							-0.903	-0.798	-0.911

Rigorous inspections of all values presented in Table 8 and Fig. 7 for the free base species, it is observed that the three types of charges follow the same behaviors in both media. In contrast, the behaviors change in the cationic and hydrochloride species. Hence, in the free base species, the Mulliken charges have different behaviors than the other ones. Thus, higher values are observed in the Mulliken charges on N3 in both media, while the MK and NPA charges show the most negative values on N3 in the two media. On the other hand, the MK

charges on C4 and C13 in both media have positive values, while the Mulliken charges in both media show for these atoms negative values. The three charges show positive values on H22. Evaluating the charges on the atoms of cationic species in the two media, it is observed that the Mulliken charges show the most negative values on C4 while the MK charges the most positive on these atoms. The NPA charges on the H22 and H31 present the most positive values than the other ones.

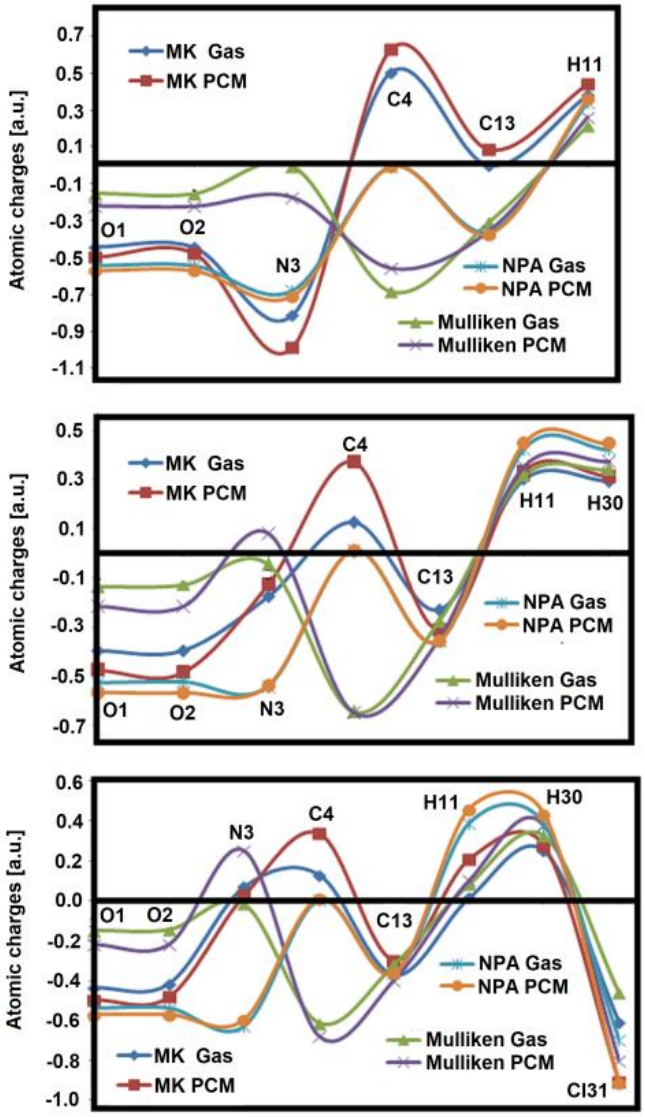

Figure 7. Behaviors of atomic MK, Mulliken, and NPA charges on the O, N, H, and Cl atoms of the free base (upper), cationic (medium), and hydrochloride (bottom) species of S(+) form of ecstasy in both media.

The three charges have different behaviors on all atoms of hydrochloride species in the two media; hence, the MK charges show the most negative values on O1, O2, C13, and Cl31 while the NPA charges on O1, O2, N3, C13, and Cl31 and the Mulliken charges show values less damaging on the O1 and O2 atoms and most negative on C4. The three charges evidence positive values on the two H atoms, although the MK charge shows practically a null value on H22 in the gas phase. These studies show that the three types of charges have a higher influence on the N atoms belonging to N-CH_3 groups of three species of S(+) form of ecstasy in both media than the O atoms of R1 ring. Besides, as mentioned above, the three ecstasy species are secondary amines where the H22 and H30 atoms are linked to N3 atoms of three species.

Molecular electrostatic potentials (MEP) were also predicted for the three species of S(+) form of ecstasy species in both media by using the B3LYP/6-311++G** level of theory.

These values are presented in Table 9, together with the bond order (BO) expressed as Wiberg indexes. As expected, the MEP values for the three species follow the tendency: Cl > O > N >C >H atoms where the most negative values are observed on the Cl atoms in both media. In contrast, the less negative ones are predicted on the H atoms because these atoms are most labile. Note that the H30 atoms of methylenedioxy groups of cationic species are the most labile in both media. Thus, in the mapped MEP surfaces of those three ecstasy species which, are presented in Figure 8, are expected strong red colors on the two O atoms of methylenedioxy ring and on the N atoms evidencing in these regions nucleophilic places where reactions with reactive potential electrophiles can occur. On the other hand, all blue color surfaces are expected on the cationic species in both media, which are typical electrophilic regions, as observed in alkaloids species [1-5,7,10] while in the free base and hydrochloride species the blue colors are easily observed on the N-H groups of methylenedioxy groups. Finally, inert regions with green colors are expected on the phenyl rings of those three species.

Table 9. Calculated molecular electrostatic potentials (a.u.) observed on some atoms of the three species of S(+) ecstasy in the gas phase and aqueous solution by using B3LYP/6-311++G** levels of theory.

Atoms	B3LYP/6-311++G**					
	Molecular electrostatic potentials					
	Gas-phase			Aqueous solution		
	Freebase	Cationic	Hydrochloride	Freebase	Cationic	Hydrochloride
1 O	-22.324	-22.228	-22.308	-22.336	-22.258	-22.317
2 O	-22.325	-22.229	-22.309	-22.337	-22.265	-22.321
3 N	-18.413	-18.101	-18.306	-18.415	-18.063	-18.244
4 C	-14.742	-14.546	-14.695	-14.742	-14.517	-14.656
13 C	-14.757	-14.549	-14.708	-14.757	-14.525	-14.673
22 H	-0.793	-1.070	-0.990	-1.060	-0.745	-0.976
30 H	-	-0.792	-0.979	-	-0.744	-0.904
31 Cl	-	-	-64.519	-		-64.565
Bond order (Wiberg Index)						
Atoms	Gas-phase			Aqueous solution		
	Freebase	Cationic	Hydrochloride	Freebase	Cationic	Hydrochloride
1 O	2.093	2.119	2.100	2.060	2.064	2.062
2 O	2.090	2.124	2.100	2.058	2.062	2.061
3 N	2.984	3.414	3.274	2.949	3.406	3.343
4 C	3.954	3.868	3.909	3.952	3.885	3.893
13 C	3.864	3.759	3.802	3.857	3.766	3.775
22 H	0.887	0.822	0.857	0.873	0.800	0.795
30 H		0.824	0.856		0.802	0.814
31 Cl			0.528			0.173

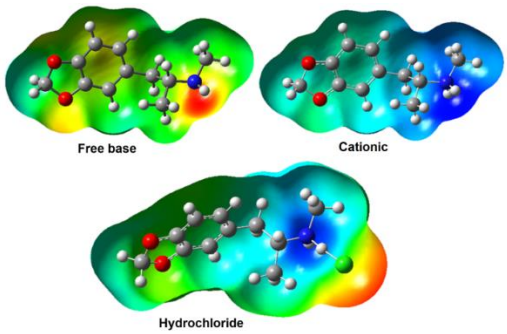

Figure 8. Calculated electrostatic potential surfaces on the molecular surfaces of the free base, cationic and hydrochloride species of S(+) form of ecstasy. Color ranges are indicated in units a.u. B3LYP functional and 6-31G* basis set. Isodensity value of 0.005.

Bond orders (BO), expressed as Wiberg indexes, are interesting parameters that predict the strength of different bonds in the different media. Here, the BO values of the O and N atoms increase in the cationic species in both media, as compared with the other two species. In

contrast, the C and H atoms in the cationic species decrease the values. These variations in the BO can be attributed to an increase of the capacity donor of H bonds of O and N atoms, which are related to the lower MEP values observed on these atoms from Table 9 and to the lower MK charges observed on the cationic species in both media.

3.4. Stability study by using NBO and AIM analyses.

The NBO 3.1 program is useful to compute the donor-acceptor energy interactions by using Second-Order Perturbation Theory Analysis of Fock Matrix in NBO Basis, expressed as E(2), as reported by Glendening et al. [69]. The total energy of these different delocalization energies can predict the stability of a species; hence, the values for the three S(+) ecstasy species can be seen in Table 10. The essential delocalization energies are observed from bonding orbitals corresponding to C=C, N-C bonds, or lone pairs of N, O, and Cl atoms to antibonding orbitals corresponding to C=C and N-H bonds. These different $\pi \rightarrow \pi^*$, $n \rightarrow \pi^*$, $n \rightarrow \sigma^*$, $\pi^* \rightarrow \pi^*$, $\sigma \rightarrow n^*$, and $n \rightarrow n^*$ transitions are similar to those observed in scopolamine species [7]. Note that the $\sigma \rightarrow n^*$ and $n \rightarrow n^*$ interactions are only observed for the hydrochloride species in the gas phase, while the *LP(4)Cl31→ σ*N3-H22* interaction is only observed for this species in solution. Hence, different behaviors are observed for the three ecstasy species in both media. Total energies are observed for the hydrochloride species in both media being higher in solution.

Table 10. Main delocalization energy (in kJ/mol) values of the three S(+) ecstasy species in the gas phase and aqueous solution by using the B3LYP/6-311++G**** level of theory.

B3LYP/6-311++G**						
Delocalization	Gas-phase			Aqueous solution		
	Freebase	Cationic	Hydrochloride	Freebase	Cationic	Hydrochloride
*πC6-C10→ π*C8-C9*	73.84	68.38	72.19	74.53	74,40	74.65
*πC6-C10→ π*C11-C12*	80.84	67.63	76.24	82.05	78,67	79.67
*πC8-C9→ π*C6-C10*	81.93	83.52	82.43	81.22	81,05	81.34
*πC8-C9→ π*C11-C12*	82.47	78.88	81.55	83.18	83,64	83.64
*πC11-C12→ π*C6-C10*	74.49	84.52	77.71	73.74	75,95	75.74
*πC11-C12→ π*C8-C9*	85.90	87.36	86.48	85.82	85,44	85.61
$\Sigma_{\pi \rightarrow \pi^*}$	**479.47**	**470.29**	**476.6**	**480.54**	**479,15**	**480.65**
*LP(2) O1→ π*C8-C9*	104.96	122.27	109.35	97.39	99,15	97.94
*LP(2) O2→ π*C11-C12*	103.41	120.05	107.64	96.22	98,77	97.31
*LP(4)Cl31→ σ*N3-H22*						111.52
$\Sigma_{n \rightarrow \pi^*}$	**208.37**	**242.32**	**216.99**	**193.61**	**197,92**	**306.77**
*π*C8-C9→ π*C6-C10*	992.67			999.48	1209,94	1179.39
*π*C11-C12→ π*C6-C10*	907.77			862.96	1077,06	1051.52
$\Sigma_{\pi^* \rightarrow \pi^*}$	**1900.44**			**1862.44**	**2287.00**	**2230.91**
σN3-C4→ LP(1)H22*			44.39			
σN3-C13→ LP(1)H22*			46.19			
$\Sigma_{\sigma \rightarrow n^*}$			**90.58**			
LP(1)N3 → LP(1)H22*			1200.1			
LP(4)Cl31 → LP(1)H22*			836.13			
$\Sigma_{n \rightarrow n^*}$			**2036.23**			
Σ_{TOTAL}	**2588.28**	**712.61**	**2820.4**	**2536.59**	**2964,07**	**3018.33**

Thus, higher energy values are predicted for the free base and hydrochloride species in the gas phase, while in solution, the cationic and hydrochloride species present higher total energies. Hence, the total energies reveal the high stability of cationic and hydrochloride forms in solution. Here, it is challenging to understand the existence of cationic form if the hydrochloride one is most stable in both media. Hence, in order to justify why these discrepancies occur, AIM calculations were also performed below.

The Bader's theory of atoms in molecules is a practical tool to predict different types of interactions knowing the topological properties through version 2000 of AIM program [70,76]. Later, the electron density, $\rho(r)$, the Laplacian values, $\nabla^2\rho(r)$, the eigenvalues of the Hessian matrix $(\lambda 1, \lambda 2, \lambda 3)$ and the $|\lambda 1|/\lambda 3$ ratio are calculated in the bond critical points (BCPs) and in the ring critical points (RCPs) for the free base, cationic and hydrochloride species of S(+) form of ecstasy. Table 11 shows these parameters for the three species in both media at the B3LYP/6-311++G** level of theory. Here, only for the hydrochloride species in the gas phase is observed an interaction of hydrogen bond C13-H27···H17 while in solution besides it is observed other ionic interaction N3-H30···Cl31 (closed-shell interaction). Hence, in both interactions $|\lambda 1|/\lambda 3 < 1$ and $\nabla^2\rho(r) > 0$ while when is covalent (shared interaction) the interaction present high $\rho(r)$ and $\nabla^2\rho(r)$ values, the ratio $\lambda 1/\lambda 3 > 1$ and $\nabla^2\rho(r) < 0$ [77]. These new H bond interactions formed in the hydrochloride species in both media can be easily seen in Figure 9. A new RCPN is formed with the C13-H27···H17 interaction, while RCP1 and RCP2 correspond to the RCPs of methylenedioxy and phenyl rings, respectively. In free base and cationic species are seen the own RCPs of two rings.

Table 11. Analyses of the Bond Critical Points (BSPs) and Ring Critical Points (RCPs) of the three S(+) ecstasy species in gas and aqueous solution phases by using the B3LYP/6-311++G****** level of theory.

Gas-phase									
Parameter[#]	Freebase		Cationic		Hydrochloride				
	RCP1	RCP2	RCP1	RCP2	RCP1	RCP2	H22-Cl31		
ρ(r)	0.0488	0.0215	0.0484	0.0214	0.0487	0.0215	0.0879		
$\nabla^2\rho(r)$	-0.33	-0.1572	-0.3312	-0.1568	-0.3304	-0.1572	0.0084		
λ1	-0.0555	-0.0159	-0.0565	-0.0157	-0.0558	-0.0159	-0.1539		
λ2	0.1810	0.0805	0.1873	0.0801	0.1828	0.0804	-0.1537		
λ3	0.2043	0.0926	0.2004	0.0923	0.2036	0.0927	0.3160		
|λ1|/|λ3|	-0.2717	-0.1717	-0.2819	-0.1701	-0.2742	-0.1715	-0.4870		
Distance							1.699		
Aqueous solution									
Parameter[#]	Freebase		Cationic		Hydrochloride				
	RCP1	RCP2	RCP1	RCP2	RCP1	RCP2	RCPN	H17-H27	H22-Cl31
ρ(r)	0.0487	0.0215	0.0476	0.0217	0.0478	0.0217	0.0108	0.0108	0.0337
$\nabla^2\rho(r)$	-0.33	-0.1572	-0.3224	-0.158	-0.3232	-0.158	-0.0468	-0.0436	-0.07
λ1	-0.0555	-0.0159	-0.0538	-0.0159	-0.0536	-0.0159	-0.0087	-0.0091	-0.0428
λ2	0.1810	0.0805	0.1784	0.0808	0.1779	0.0806	0.0022	-0.0020	-0.0427
λ3	0.2043	0.0926	0.1979	0.093	0.1988	0.0932	0.0535	0.0549	0.1555
|λ1|/|λ3|	-0.2717	-0.1717	-0.2719	-0.171	-0.2696	-0.1706	-0.1626	-0.1658	-0.2752
Distance									2.092

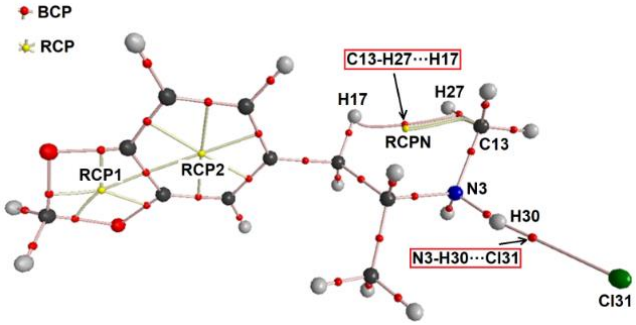

Figure 9. Molecular graphic for the hydrochloride species of S(+) ecstasy in aqueous solution showing the geometry of all their critical bond points (BCPs) and ring critical points (RCPs) by using the B3LYP/6-311++G** method.

Here, it is essential to observe that the H22···Cl31 distance notably increases in solution, as a consequence of the hydration. The formation of two new H bond interactions

supports the high stability of hydrochloride species in solution in accordance with the NBO studies. But, the N3-H30···Cl31 is ionic, indicating, in this case, the formation of the cation.

3.5. Frontier orbitals and global descriptors studies.

To investigate the chemical reactivity and kinetic stability of a species, Parr and Pearson have suggested calculating both frontier orbitals and their differences named gap [55,56]. Later, a series of global descriptors can be computed with these gap values using known equations reported in the literature [57-65]. Hence, for the three S(+) ecstasy species in both media, the highest occupied molecular orbital (HOMO) and the lowest unoccupied molecular orbital (LUMO) were computed together with the chemical potential (μ), electronegativity (χ), global hardness (η), global softness (S), global electrophilicity index (ω) and global nucleophilicity index (E) descriptors in order to predict their reactivities and behaviors in both media. Thus, the results for the three species in the two media and by using the B3LYP/6-311++G** level of theory are presented in Table 12. Analyzing the gap values, we observed that the cationic species is the most reactive in both media because its species has the lowest gap value, as expected because it charged species is the most unstable while the reactivity of free base increases in solution due to the protonation of >N-CH_3 group. On the contrary, the reactivity of hydrochloride form is less reactive in solution, in accordance with its higher stability evidenced by AIM and NBO calculations in this medium.

Table 12. Frontier orbitals, gap values, and global descriptors for the three S(+) ecstasy species in the gas phase and aqueous solution by using the B3LYP/6-311++G****** level of theory.

Gas-phase			
Orbitals (eV)	Freebase	Cationic	Hydrochloride
HOMO	-5.8504	-8.6342	-6.2559
LUMO	-0.4762	-4.7130	-0.9878
|GAP|	5.3742	3.9212	5.2681
Descriptors			
χ	-3.1633	-1.9606	-2.6341
μ	-2.6871	-6.6736	-3.6219
η	3.1633	1.9606	2.6341
S	0.1581	0.2550	0.1898
ω	1.1413	11.3582	2.4900
E	-8.500	-13.084	-9.540
Aqueous solution			
Orbitals (eV)	Free base	Cationic	Hydrochloride
HOMO	-5.9104	-5.9076	-5.9893
LUMO	-0.4762	-0.4762	-0.5361
|GAP|	5.4342	5.4314	5.4532
Descriptors			
χ	-2.7171	-2.7157	-2.7266
μ	-3.1933	-3.1919	-3.2627
η	2.7171	2.7157	2.7266
S	0.1840	0.1841	0.1834
ω	1.8765	1.8758	1.9521
E	-8.676	-8.668	-8.896

χ = - [E(LUMO)- E(HOMO)] /2; = [E(LUMO) + E(HOMO)] /2; = [E(LUMO) - E(HOMO)] /2; S = ½η; ω = $\mu^2/2\eta$ E=m*h

Probably, the high values of global electrophilicity index (ω) and global nucleophilicity index (E) in the gas phase justify the low gap value of cationic species in this medium while the lower value in solution could be justified by the lower values of those two indexes, as observed in Table 12. When the gap values for the three ecstasy species are compared in Table 13 and Figure 10 with those reported for heroin, morphine, cocaine, tropane, scopolamine and 2-CB alkaloids in both media by using B3LYP/6-31G* basis set [1-3,5,7,10] we observed that

the free base of cocaine in both media have the low gap values and, hence, this species is the most reactive and, then, the species of ecstasy is the most reactive in the two media. Analyzing the gap values for the cationic species, the species of ecstasy is the most reactive in the gas phase (3.9212 eV), while in solution, the species of morphine is the most reactive. The gap value for the cationic species of 2-CB was not presented because the B3LYP/6-31G*calculation has optimized this species with an imaginary frequency. If now are evaluated, the hydrochloride/hydrobromide the cocaine species is the most reactive in both media. Note that the three tropane species have low reactivities in the two media and are the less reactive, having its cationic species the highest gap value (9.5595 eV). The behaviors of gap values in the three species of ecstasy are practically similar to those corresponding to scopolamine.

Table 13. Gap values for the three S(+) ecstasy species in the gas phase and aqueous solution by using the B3LYP/6-311++G** level of theory.

Species	B3LYP Method					
	Freebase		Cationic		Hydrochloride	
	Gas	PCM	Gas	PCM	Gas	PCM
Heroin[b]	5.6563	5.6414	5.4268	5.3757	4.4469	5.3024
Morphine[c]	5.6044	5.475	5.1889	5.0244	4.584	5.4417
Cocaine[d]	4.858	4.9487	5.4468	5.466	3.6813	4.5082
Tropane[e]	7.5506	7.6611	9.5595	9.525	5.9119	6.8246
Scopolamine[f]	5.4004	5.4758	5.6356	5.6289	5.4026	4.9239
Ecstasy[a]	5.3742	5.4342	3.9212	5.4314	5.4532	5.2681
2-CB[g]	5.4613	5.4804	4.4055	#	3.8178	5.513

[a]This work, [b]from ref [5], [c]from ref [1], [d]from ref [3], [e]from ref [2], [f]from ref [7], [g]from ref [10], [#]Imaginary frequencies

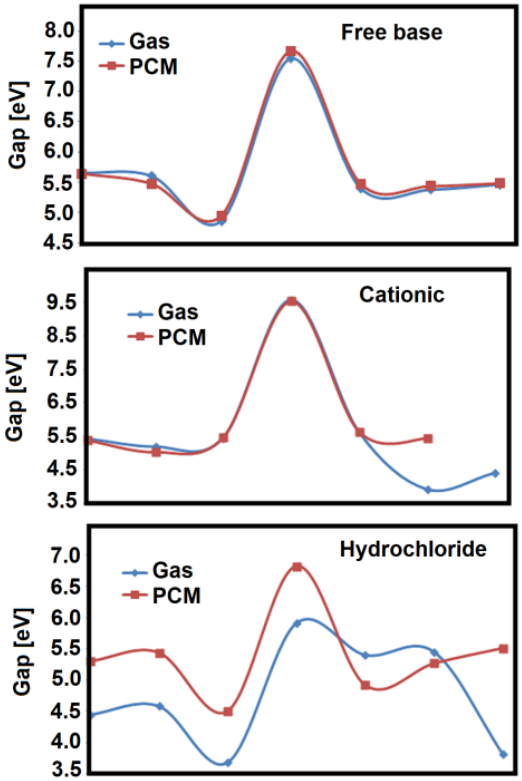

Figure 10. Gap values for the hydrochloride species of S(+) ecstasy in the gas phase and aqueous solution by using the B3LYP/6-311++G** method compared with the corresponding to alkaloids species in both media by using B3LYP/6-31G* level of theory.

These studies show that all hydrochloride/hydrobromide forms are the most reactive species in solution, except for morphine, probably because they have higher solvation energies (between -162 and -122 kJ/mol), as compared with the free base species

3.6. NMR study.

The predicted ^{1}H- and ^{13}C-NMR chemical shifts in aqueous solution calculated by using the GIAO method [73] and the B3LYP/6-311++G** level of theory are compared with the available experimental ones in $CDCl_3$ taken from the literature [27,40-42] in Table 14 together with the corresponding RMSD values. Good correlations are observed between the predicted chemical shifts and the experimental ones of three specie with RMSD values for the ^{1}H nucleus between 0.4 and 0.3 ppm. On the contrary, the RMSD values slightly increase between 19.9 and 3.6 ppm for the ^{13}C nucleus, where the higher value presents the hydrochloride form probably due to that its cationic species is present in solution. In general, the theoretical values are overestimated about the experimental ones.

Table 14. Observed in $CDCl_3$ and calculated ^{1}H and ^{13}C chemical shifts (δ in ppm) for the three ecstasy species in aqueous solution by using the B3LYP/6-311++G****** level of theory.

Atoms		^{1}H-RMN[a]			Exp[b]
		Freebase	Cationic	HCl	
15	H	2.3	3.3	3.0	
16	H	1.8	2.2	2.1	2.7
17	H	3.1	3.4	3.3	2.7
18	H	0.8	1.2	0.9	1.1
19	H	1.2	1.3	1.1	1.1
20	H	0.8	1.2	1.6	1.1
21	H	7.0	7.0	6.9	6.8
22	H	0.7	4.5	10.4	
23	H	6.9	7.0	7.0	6.7
24	H	7.0	7.1	7.1	6.7
25	H	2.3	2.8	2.4	2.6
26	H	2.6	3.1	2.9	2.6
27	H	2.7	3.2	2.9	2.6
28	H	6.1	6.2	5.8	6.0
29	H	5.8	5.8	6.2	6.0
30	H	-	4.1	3.3	
RMSD		**0.3**	**0.4**	**0.3**	
Atoms		^{13}C-RMN			Exp[c]
4	C	66.2	66.5	81.6	59.3
5	C	43.8	39.8	57.5	41.3
6	C	142.9	136.3	155.0	132.3
7	C	20.2	18.6	34.5	17.7
8	C	116.1	116.4	133.6	112.5
9	C	154.1	154.6	172.1	150.3
10	C	127.4	127.8	145.3	125.7
11	C	152.1	153.7	171.1	149.1
12	C	113.2	113.5	131.0	111.6
13	C	36.0	34.5	49.7	32.8
14	C	105.7	106.1	123.0	104.0
RMSD		**4.5**	**3.6**	**19.9**	

[a]This work GIAO/B3LYP/6-311++G** Ref. to TMS, [b]From Ref [40-42], [c]From Ref [27,42].

3.7. Vibrational study.

B3LYP/6-311++G** calculations have optimized the three species of S(+) ecstasy with *C1* symmetries and, as the free base, cationic and hydrochloride species have respectively 29, 30 and 31 atoms in its structures the expected normal vibration modes are 81, 84 and 87 and, where all modes are active in both IR and Raman spectra. Figures 11 and 12 show comparisons between the experimental available attenuated total reflectance ATR-IR and FT-Raman spectra, respectively, for the hydrochloride species of ecstasy [20,28,29,33,52] with the corresponding predicted for the free base, cationic and hydrochloride species in the gas phase at the B3LYP/6-311++G** level of theory.

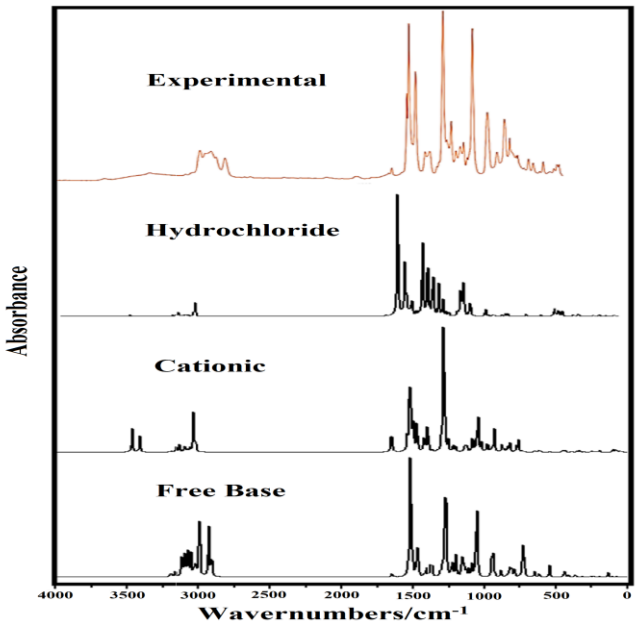

Figure 11. Experimental infrared spectrum of hydrochloride ecstasy compared with the corresponding predicted for the free base, cationic, and hydrochloride species by using B3LYP/6-311++G** level of theory.

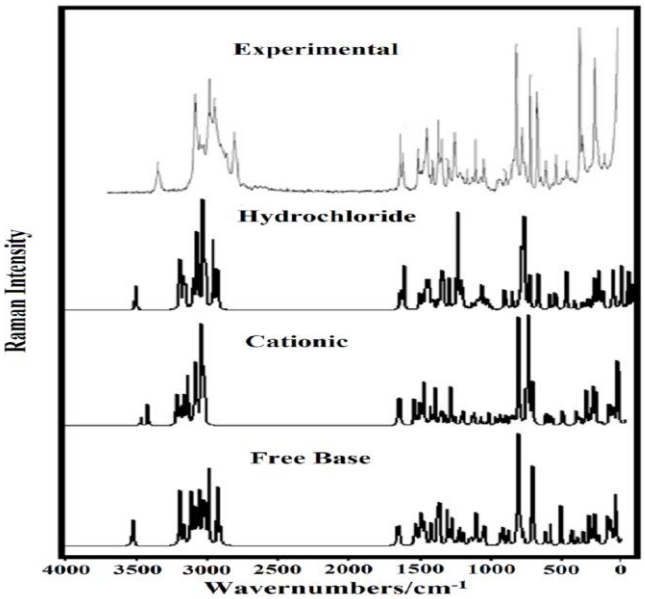

Figure 12. Experimental Raman spectrum of hydrochloride ecstasy species compared with the corresponding predicted for the free base, cationic, and hydrochloride species by using B3LYP/6-311++G** level of theory.

The SQMFF methodology and the Molvib program, together with the normal internal coordinates and scaling factors, were employed to obtain the harmonic force fields of three ecstasy species [49-51]. Later, the complete assignments of all bands observed in the experimental vibrational spectra were performed using potential energy distributions (PED) contributions ≥ 10 %. Table 15 is given observed and calculated wavenumbers and assignments for the free base, cationic, and hydrochloride species of ecstasy in the gas phase. The rigorous examinations of both spectra show the probable presence of three species in the solid phase quickly because the three very intense IR bands at 1496, 1253, and 1042 cm^{-1} are assigned to vibration modes of three species while in the corresponding predicted spectra only two strong bands are observed. Note that the two anti-symmetric and symmetric NH_2 stretching modes of cationic and hydrochloride species of ecstasy are predicted at higher wavenumbers and observed respectively as weak bands in the IR and Raman spectra between 3327 and 3330 cm^{-}

[1]. On the other hand, the experimental IR band at 2794 cm^{-1} can be assigned to the symmetric mode of CH_3 group corresponding to the free base because the SQM calculations predict this mode only for this species at 2795 cm^{-1}. Besides, the aliphatic the C4-H15 stretching mode for the free base species is predicted at 2774 $cm^{-1,}$ while for the other two species, these modes are predicted at higher wavenumbers. Better correlations are observed in the Raman spectra in the region of higher wavenumbers when the corresponding spectrum predicted in activities were transformed into intensities by using known equations [71,72]. Discussions of some assignments are presented by the regions below.

Table 15. Observed and calculated wavenumbers (cm^{-1}) and assignments for the three S(+) ecstasy species in gas and aqueous solution phases by using the B3LYP/6-311++G** level of theory.

Experimental		B3LYP/6-311++G** method					
		Freebase		Cationic		Hydrochloride	
IR[c]	Ra[d]	SQM[b]	Assignments[a]	SQM	Assignments[a]	SQM[b]	Assignments[a]
3327w	3330w	3367	νN3-H22	3322	ν_aNH_2	3327	ν_aNH_2
3327w	3330w			3274	ν_sNH_2		
3073vw	3070s	3053	νC12-H24	3077	νC12-H24	3072	νC12-H24
		3044	νC8-H21	3057	νC8-H21	3059	νC8-H21
3030sh	3037m	3021	νC10-H23	3052	ν_aCH_3(C13)	3037	νC10-H23
	3000w	2978	ν_aCH_2(C14)	3034	ν_aCH_3(C13)	3016	ν_aCH_3(C13)
2969m	2968s	2967	ν_aCH_3(C7)	3030	νC10-H23	3012	ν_aCH_3(C13)
		2953	ν_aCH_3(C13)	3004	ν_aCH_2(C14)	3000	ν_aCH_3(C7)
		2937	ν_aCH_3(C7)	3002	ν_aCH_3(C7)	2997	ν_aCH_2(C14)
		2933	ν_aCH_2(C5)	2970	ν_aCH_3(C7)	2972	ν_aCH_3(C7)
		2916	ν_aCH_3(C13)	2954	νC4-H15	2949	ν_aCH_2(C5)
2933m	2933s	2896	ν_sCH_2(C5)	2951	ν_sCH_3(C13)	2933	ν_sCH_3(C13)
2894m	2875sh	2881	ν_sCH_3(C7)	2938	ν_aCH_2(C5)	2931	νC4-H15
2865sh	2849sh	2857	ν_sCH_2(C14)	2915	ν_sCH_2(C14)	2896	ν_sCH_2(C5)
2794m	2794m	2795	ν_sCH_3(C13)	2903	ν_sCH_3(C7)	2895	ν_sCH_3(C7)
2794m	2794m	2774	νC4-H15	2895	ν_sCH_2(C5)	2882	ν_sCH_2(C14)
1615w	1629s	1605	νC8-C9	1601	νC9-C11	1605	νC8-C9
	1609m	1591	νC11-C12	1590	νC11-C12	1593	νC11-C12
1508s	1502m			1578	δNH_2	1522	ν_sNH_2
1496vs		1476	δCH_2(C14)	1479	δCH_2(C14)	1477	δCH_2(C14)
	1468sh	1473	βN3-H22	1469	δCH_2(C14)	1467	δCH_2(C14)
	1456sh	1466	δCH_2(C14)			1454	δ_aCH_3(C13)
1448s	1442s	1445	δ_aCH_3(C13)	1445	δ_aCH_3(C13)	1453	δ_aCH_3(C13)
	1436sh	1438	δ_aCH_3(C7)	1443	δ_aCH_3(C7)	1444	δ_aCH_3(C7)
		1432	δ_aCH_3(C7)	1437	δ_aCH_3(C13)	1441	δ_aCH_3(C7)
		1426	δCH_2(C5)	1432	δ_aCH_3(C7)	1432	δ_aCH_3(C13)
1428sh		1423	δ_aCH_3(C13)	1430	νC10-C12	1427	δ_aCH_3(C13)
		1420	δCH_2(C5)	1415	δCH_2(C5)	1422	δCH_2(C5)
				1408	$wagCH_2$(C14)	1413	δ_sCH_3(C13)
		1404	$wagCH_2$(C14)	1400	δ_sCH_3(C13)	1406	$wagCH_2$(C14)
				1393	$wagNH_2$	1392	ρNH_2
	1398w	1395	δ_sCH_3(C13)	1367	δ_sCH_3(C7)	1364	δ_sCH_3(C7)
1377w	1360s	1355	δ_sCH_3(C7)	1362	δ_sCH_3(C7)	1352	δ_sCH_3(C13)
1345w	1337s	1340	ρ'C4-H15	1351	νC6-C10	1343	νC6-C10
	1337s	1335	δ_sCH_3(C7)	1337	$wagCH_2$(C5)	1321	ρ'C4-H15
	1329sh	1323	νC6-C10	1321	ρ'C4-H15	1307	ρC4-H15
1293sh	1280w	1284	$wagCH_2$(C5)	1290	ρC4-H15	1291	$wagCH_2$(C5)
1273sh		1265	βC8-H21	1268	βC8-H21	1269	βC8-H21
1253vs	1247s	1234	νC10-	1244	νC10-C12	1238	νO1-C9
1226sh	1200w	1198	ρ'CH_3(C13)				
		1197	ρCH_2(C5)	1215	ρCH_2(C5)	1209	ρCH_2(C5)
1194m		1192	ρCH_2(C14)	1190	βR_1(A1)	1193	νO2-C11
1166w	1155w	1169	ρCH_2(C14)	1173	ρCH_2(C14)	1179	ρCH_2(C14)
1138sh		1121	ρCH_3(C13)	1166	ρ'CH_3(C13)	1171	ρCH_2(C14)
1130w	1115w	1111	βC12-H24	1119	βC12-H24	1114	βC12-H24
1106w	1098s	1096	ρCH_3(C13)	1103	ρCH_3(C13)	1089	βR_1(A1)
1078sh	1070w	1082	βR_1(A1)	1094	νO1-C9	1085	ρCH_3(C13)

Experimental		B3LYP/6-311++G** method					
		Freebase		Cationic		Hydrochloride	
IR[c]	Ra[d]	SQM[b]	Assignments[a]	SQM	Assignments[a]	SQM[b]	Assignments[a]
1062sh		1057	ρ'CH_3(C13)	1053	ρCH_3(C7)	1071	ρ'CH_3(C13)
1042vs	1042m	1042	τwCH_2(C14)	1040	νC4-C7	1055	νC4-C7
		1035	τwCH_2(C14)	1027	τwCH_2(C14)	1037	τwCH_2(C14)
		1024	νC4-C7	1005	τwCH_2(C14)	1018	ρ'CH_3(C7)
	1000w	1008	τwCH_2(C14)	998	ρ'CH_3(C7)	1008	τwCH_2(C14)
947sh		929	γC10-H23	942	νN3-C13	1005	νN3-C13
939m		917	νO1-C9	927	γC12-H24	930	γC10-H23
	910w	913	νO1-C14	922	νO1-C9	920	νO1-C9
875w	887w	900	ρCH_3(C7)	904	νO1-C14	911	νO1-C14
	850sh	872	γC8-H21	872	νC4-C5	886	νC4-C5
	843sh	842	ρ'CH_3(C7)	856	γC8-H21	866	γC8-H21
816m	813vs	819	γC12-H24	818	γC10-H23	844	νN3-C4
				809	τwCH_2(C5)	824	τwCH_2(C5)
		798	νO2-C11	805	γC10-H23	812	γC12-H24
	772s	784	τwCH_2(C5)	787	τwNH_2	796	νC9-C11
776w		774	βR_1(A2)	748	νN3-C4	770	νN3-C4
730sh		722	βR_2(A2)	725	τwNH_2	764	τwNH_2
680vw	715vs	714	γN3-H22	724	βR_2(A2)	723	βR_2(A2)
644w	667s	713	τR_1(A1)	706	τR_1(A1)	709	τR_1(A1)
613w	650w	636	βR_1(A2)	632	βR_1(A2)	642	βR_1(A2)
606w	604m	602	τR_3(A1)	599	γC6-C5	598	τR_3(A1)
540w	535w	535	βR_3(A1)	531	βR_3(A1)	540	βR_3(A1)
463vw	457w	475	δC7C4N3	446	δC5C4C7	456	δC5C4C7
439w		438	βR_2(A1)	438	βR_2(A1)	445	βR_2(A1)
425w	425w	426	τR_2(A1)	418	τR_2(A1)	430	τR_2(A1)
409sh	393sh	394	δC5C4C7	379	δC5C4C7	414	τR_2(A1)
	370vs	357	δC4N3C13	346	δC4N3C13	387	τR_2(A1)
	358s	325	ButtC11-C9	321	ButtC11-C9	325	τwC5-C6
	350sh	300	βC6-C5	289	βC6-C5	305	δC4N3C13
	266vs	239	τR_2(A2)	232	ButtC11-C9	279	βC6-C5
	250sh	227	βC6-C5	222	τwCH_3(C7)	239	τR_2(A2)
	238sh	211	τwCH_3(C7)	205	τwCH_3(C7)	221	τwCH_3(C7)
	202w	192	τR_3(A1),	185	τR_3(A1)	193	τR_3(A1)
						186	δC5C4N3
	139sh	185	τwCH_3(C13)	175	τwCH_3(C13)	170	τwCH_3(C13)
	127sh	133	τR_1(A2)			133	τR_1(A2)
	115sh					128	δN3H22Cl31
	103vs			97	τR_1(A2),τR_2(A2)	86	τN3-H22
	91vs	95	τN3-C4	72	τN3-C4		
		69	γC6-C5	65	δC6C5C4	65	τN3-C4
		41	τC4-C5	42	τwC5-C6	35	τC4-C5
		27	τwC5-C6	26	τC4-C5	27	τC4-C5
						22	τwC5-C6

Abbreviations: ν, stretching; wag, wagging; τ, torsion; ρ, rocking; τw, twisting; δ, deformation; a, antisymmetric; s, symmetric; (A_1), Ring R1; (A_2), Ring R2; [a]This work, [b]From scaled quantum mechanics force field B3LYP/6-311++G** method; [c]From Ref [52]; [d]From Ref [28,29,33].

3.7.1. 4000-2000 cm^{-1} region.

In this region are expected the CH_3, CH_2, and NH_2 anti-symmetric and symmetric stretching modes corresponding to the three species and the aromatic and aliphatic C-H stretching modes. The IR band at 3327 cm^{-1} is assigned to the N3-H22 stretching mode of the free base and to the two NH_2 stretching modes expected for the cationic and hydrochloride species because of the SQM calculations predicted these modes in that region.

The group of IR and Raman bands between 3073 and 2794 cm^{-1} is assigned as predicted by SQM calculations to CH_3, CH_2, and NH_2 anti-symmetric modes. Symmetric stretching modes corresponding to the three species and to aromatic and aliphatic C-H stretching modes

are assigned, as detailed in Table 15. Here, the IR band of medium intensity at 2794 cm^{-1} can be assigned to symmetric CH_3 and C4-H15 stretching modes of the free base because the SQM calculations predicted these modes respectively at 2795 and 2772 cm^{-1}. The Raman bands and shoulders between 2933 and 2794 cm^{-1} are assigned to symmetric CH_2 stretching modes, as predicted by calculations and as were assigned in similar species [1-3,7,10,11-19].

3.7.2. 2000-1000 cm^{-1} region.

The strong IR and Raman bands between 1629 and 1502 cm^{-1} are assigned to the expected C=C stretching modes corresponding to R2 ring while the IR band at 1508 cm^{-1} that appear with medium intensity in Raman at 1502 cm^{-1} is assigned to NH_2 stretching mode of hydrochloride species and to NH_2 deformation modes of cationic species, as predicted by SQM calculations. Then, the very intense IR band at 1496 cm^{-1} is independently assigned to CH_2 deformations modes or C9=C11 stretching modes commons to both R1 and R2 rings of three species [1-3,7,10]. The strong IR band at 1448 cm^{-1} can be simultaneously assigned to CH_3 and CH_2 deformation modes of three species or NH_2 deformation or wagging NH_2 modes of hydrochloride species. On the other hand, the very intense IR bands at 1253 and 1042 cm^{-1} can be assigned to C10-C12, O1-C9, or C4-C7 stretching modes of three species or CH_3 rocking and CH_2 twisting modes of free base species. The group of IR and Raman bands and shoulders between 1444 and 1000 cm^{-1} can be attributed to three C-H in-plane deformation modes of R2 ring, wagging and rocking modes of CH_3 and CH_2 groups and rocking modes of aliphatic C4-H15 groups of three species of ecstasy, as predicted by calculations and as is perfectly detailed in Table 15.

3.7.3. 1000-20 cm^{-1} region.

In this region, the C-H out-of-plane deformation (γC-H), twisting CH_3, CH_2 and NH_2 modes, C-N, O-C, and C-C stretching modes and deformations (β_R) and torsion (τ_R) modes of two R1 and R2 rings corresponding to the three species are expected. Here, these modes are assigned, taking into account the frequencies predicted by SQM calculations and according to assignments reported for species containing similar groups [1-3,7,10,11-19, 60-62,64], as is detailed in Table 15.

3.8. Force constants.

The scaled internal force constants for the three species of S(+) ecstasy calculated by using the B3LYP/6-311++G** level of theory with the SQMFF methodology and the Molvib program [49-51] are presented in Table 16 together with the reported for scopolamine alkaloid and psychotropic agent 2-CB [7,10]. When the force constants are compared for the three species, it is observed that the *f(νN-H)*, *f(νN-*CH_3*)* and *f(νC-N)* constants decrease its values in the cationic and hydrochloride species due to incorporations of H atoms in the cationic species and Cl atom in the hydrochloride one. A similar effect can be seen in 2-CB and in the hydrobromide scopolamine species when the Br atom is added to cationic species [7,10]. Note that the free base of scopolamine species does not present an N-H bond because this tertiary amine contains the >N-$(CH_3)_2$ group, while the species of 2-CB is a primary amine (C-N-H_2) and of ecstasy is a secondary amine (HN-$(CH_3)_2$). Then, the structural differences between the ecstasy and scopolamine species also affect *f(νC-N)* constants decreasing the values in the corresponding cationic and hydrochloride/hydrobromide species. The *f(ν*CH_2*)* and

*f(νCH₃)*force constant values present approximately similar values in ecstasy and in the compared species.

Table 16. Scaled internal force constants for the free base, cationic, and hydrochloride species of S(+) ecstasy in the gas phase and in aqueous solution by using the B3LYP/6-311++G** method.

Force constant	B3LYP/6-311++G** method			B3LYP/6-31G*					
	S(+) Ecstasy[a]			Scopolamine[b]			2-CB[c]		
	Freebase	Cationic	HCl	Freebase	Cationic	HBr	Freebase	Cationic	HCl
f(νN-H)	6.29	6.04	4.19		6.04	2.81	6.24	6.10	4.35
f(νN-CH₃)	4.69	3.95	4.33	4.76	3.93	3.71	3.59	3.16	4.50
f(νC=C)	6.42	6.42	6.43						
f(νC-O)$_{R2}$	4.74	4.87	4.78	3.99	4.11	3.99	5.41	5.25	5.40
f(νC-N)	4.48	2.94	3.85	4.27	3.20	3.72			
f(νCH₂)	4.69	4.76	4.73	4.82	4.85	4.84	4.79	4.91	4.84
f(νCH₃)	4.67	4.91	4.87	4.81	5.11	5.09	4.76	4.92	4.86
f(νC-H)$_{R2}$	5.07	5.12	5.12	5.14	5.15	5.15	5.24	5.25	5.24
f(νC-H)	4.26	4.81	4.74	4.84	4.85	4.86			
f(νC-C)	3.94	3.98	3.97	3.91	3.89	3.91			
f(δCH₂)	0.75	0.75	0.75	0.76	0.76	0.76	0.78	0.78	0.78
f(δCH₃)	0.54	0.54	0.54	0.58	0.56	0.56	0.59	0.58	0.59

Units are mdyn Å^{-1} for stretching and mdyn Å rad^{-2} for angle deformations, [a]this work, [b]from ref. [7], [c]from ref. [10].

3.9. Electronic circular dichroism (ECD) and Ultraviolet-visible spectra.

The ultraviolet-visible spectra of the free base, cationic, and hydrochloride species of S(+) and R(-) forms of ecstasy were predicted in aqueous solution by using TDDFT calculations and the B3LYP/6-311++G** method. These spectra are presented In Figure 13, while the predicted electronic circular dichroism spectra (ECD) for the three species of S(+) and R(-) forms are presented in Figure 14.

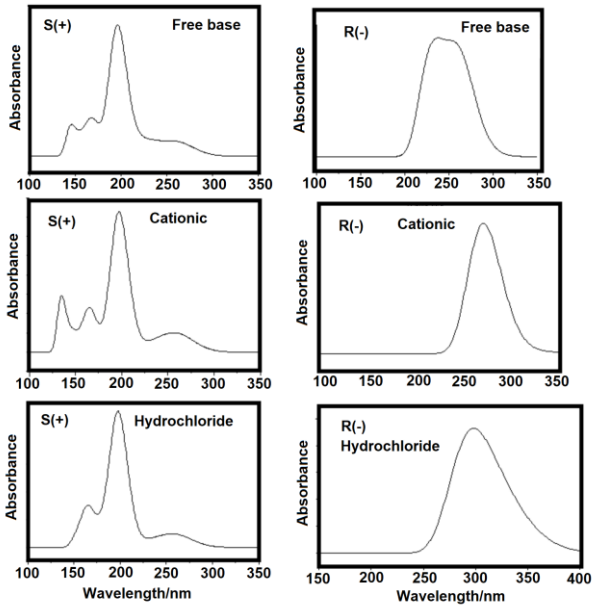

Figure 13. Predicted ultraviolet-visible spectra of the free base, cationic, and hydrochloride species of S(+) and R(-) forms of ecstasy in aqueous solution by using B3LYP/6-311++G** level of theory.

In the electronic spectra of the free base and cationic species are observed three bands and a shoulder while in the spectrum of hydrochloride species are observed two bands and a shoulder. Thus, in the free base, the bands are located at 146.5, 168.3, and 196.3 nm while the shoulder at 260 nm. In the cationic species, the three bands are at 135.5, 164.4, and 197.2 nm, and the shoulder is located at 257.6 nm. In the hydrochloride species, the two bands are observed at 164.9 and 197.7 nm while the shoulder at 257.6 nm. In the predicted UV-Vis of

three species of R(-) form, only an intense band is observed, which is located in the free base at 237 nm while in the cationic and hydrochloride species at 269.6 and 298.4 nm, respectively. The bands of intensities maxima in both forms can be assigned to $\pi \rightarrow \pi^*$ transitions which usually are observed between 210-230 nm and are attributed to C=C groups [57,60].

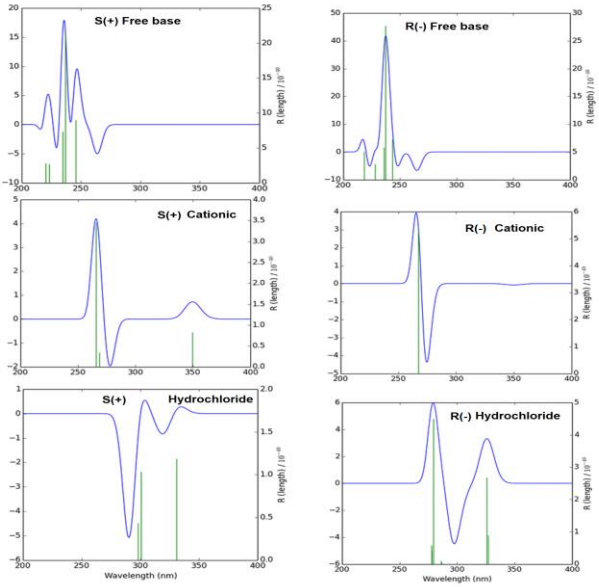

Figure 14. Predicted electronic circular dichroism spectra of the free base, cationic, and hydrochloride species of S(+)and R(-) forms of ecstasy in aqueous solution by using B3LYP/6-311++G** level of theory.

The shoulders observed in the three species of S(+) form are probably related to three species of R(-) form because these forms are quickly bio-transformed to the S(+) form, as suggested by Johnson et al. [53]. The free base is protonated in solution while the hydrochloride form is as cationic one; hence, both species are as cationic in solution. The other bands of low intensities observed in the three species of S(+) form could be associated with $n \rightarrow \pi^*$ transitions, which are also predicted by NBO calculations. The ECD spectra of three species of R(-) form show that the positions of negative bands are those observed as maxima in the UV-Vis spectra for the free base, cationic, and hydrochloride species at 237, 270 and 300 nm, respectively. The ECD spectra of three S(+) forms show the presence of negative bands corresponding to the R(-) forms; hence, in solution, the presence of racemic mixture can be predicted when the rotatory strength for the three are graphed in Figure 14.

4. Conclusions

In this work, the structures of the free base, cationic, and hydrochloride species of S(+) and R(-) enantiomers of ecstasy have been theoretically determined in the gas phase and aqueous solution by using B3LYP/6-311++G** calculations. On the other hand, the bands observed in the experimental available attenuated total reflectance ATR-IR and FT-Raman spectra were assigned entirely by using the scaled quantum mechanical force field (SQMFF) approach and the Molvib program. SQM calculations predicted that the three species could be present in the IR spectrum in the solid phase because the IR bands of medium intensity at 2794 cm^{-1} is assigned to the stretching C4-H15 and symmetric CH_3 modes of the free base while the strong IR band at 1508 cm^{-1} is assigned easily to the NH_2 deformation modes of cationic and hydrochloride species. The calculations reveal the same energy values for both enantiomers, indicating that they could exist simultaneously in the two media with similar corrected

solvation energies in solution probably because the R(-) form is quickly converted to the S(+) one. Three types of charges studied in both media evidence higher effect on the N atoms belonging to N-CH_3 groups of three species of S(+) form of ecstasy in both media than on the O atoms of R1 ring. The high gap value predicted for the hydrochloride species of S(+) form in solution, about other ones, support the low reactivity of this species, in agreement to its higher stability evidenced in this medium by AIM and NBO calculations. The predicted Ultraviolet-visible and Electronic Circular Dichroism ecstasy (ECD) support the presence of both enantiomeric forms in solution. The predicted ^{1}H- and ^{13}C-NMR chemical shifts for the three species of S(+) form of ecstasy show excellent concordance with the corresponding experimental ones.

Funding

This research received no external funding.

Acknowledgments

This work was supported with grants from CIUNT Project Nº 26/D608 (Consejo de Investigaciones, Universidad Nacional de Tucumán, Argentina). The author would like to thank Prof. Tom Sundius for his permission to use MOLVIB.

Conflicts of Interest

The authors declare no conflict of interest.

References

1. Brandán, S.A. Why morphine is a molecule chemically powerful. Their comparison with cocaine. *Indian Journal of Applied Research* **2017**, *7*, 511-528.
2. Rudyk, R.A.; Brandán, S.A. Force field, internal coordinates and vibrational study of alkaloid tropane hydrochloride by using their infrared spectrum and DFT calculations. *Paripex A Indian Journal of Research* **2017**, *6*, 616-623.
3. Romani, D.; Brandán, S.A. Vibrational analyses of alkaloid cocaine as free base, cationic and hydrochloride species based on their internal coordinates and force fields. *Paripex A Indian Journal of Research* **2017**, *6*, 587-602.
4. Iramain, M.A.; Ledesma, A.E.; Brandán, S.A. Analyzing the effects of halogen on properties of a halogenated series of R and S enantiomers analogues alkaloid cocaine-X, X=F, Cl, Br, I. *Paripex A Indian Journal of Research*, **2017**, *6*, 454-463.
5. Brandán, S.A. Understanding the potency of heroin against to morphine and cocaine. *IJSRM, International Journal of Science and Research Methodology* **2018**, *12*, 97-140.
6. Rudyk, R.A.; Checa, M.A.; Guzzetti, K.A.; Iramain, M.A.; Brandán, S.A. Behaviour of N-CH_3 Group in Tropane Alkaloids and correlations in their Properties. *IJSRM, International Journal of Science And Research Methodology* **2018**, *10*, 70-97.
7. Rudyk, R.A.; Checa, M.A.; Catalán, C.A.N.; Brandán, S.A. Structural, FT-IR, FT-Raman and ECD spectroscopic studies of free base, cationic and hydrobromide species of scopolamine alkaloid. *J. Mol. Struct.* **2019**, *1180*, 603-617, https://doi.org/10.1016/j.molstruc.2018.12.040.
8. Iramain, M.A.; Brandán, S.A. Structural and vibrational properties of three species of anti-histaminic diphenhydramine by using DFT calculations and the SQM approach. *Journal: To Chemistry Journal* **2018**, *1*, 105-130.
9. Márquez, M.J.; Iramain, M.A.; Brandán, S.A. *Ab-initio* and Vibrational studies on Free Base, Cationic and Hydrochloride Species Derived from Antihistaminic Cyclizine agent. *International Journal of Science and Research Methodology* **2019**, *11*, 53-87.
10. Manzur, M.E.; Rudyk, R.A.; Brandán, S.A. Evaluating properties of free base, cationic and hydrochloride Species of potent psychotropic 4-Bromo-2,5-dimethoxyphenethylamine drug. *International Journal of Current Advanced Research* **2019**, *8*, 17166-17170.

11. Iramain, M.A.; Ruiz Hidalgo, J.; Brandán, S.A. Predicting properties of species derived from N-(1H-indol-3-ylmethyl)-N,N-dimethylamine, Gramine, a indol alkaloid. *International Journal of Current Advanced Research* **2019**, *8*, 18113-18124.
12. Romani, D.; Ruiz Hidalgo, J.; Iramain, M.A.; Brandán, S.A., Structures, Reactivities and Vibrational Study of Species Derived from the Adrenergic α_2 Receptor Agonist Guanfacine. *International Journal of Science And Research Methodology* **2019**, *12*, 74-98.
13. Manzur, M.E.; Brandán, S.A. S(-) and R(+) Species Derived from Antihistaminic Promethazine Agent: Structural and Vibrational Studies. *Heliyon* **2019**, *5*, https://doi.org/10.1016/j.heliyon.2019.e02322.
14. Márquez, M.J.; Brandán, S.A. DFT study of Species Derived from the Narcotic Antagonist Naloxone, *Biointerface Research in Applied Chemistry* **2020,** *10*, 8096-8116, https://doi.org/10.33263/BRIAC102.096116.
15. Ruiz Hidalgo, J.; Iramain, M.A.; Brandán, S.A. Structural Studies and Spectroscopic properties of Quinolizidine Alkaloids (+) and (-)-Lupinine in different media, *J. Mater. Environ. Sci.*, **2019**, *10(9)*, 854-871.
16. Contreras, C.D.; Ledesma, A E.; Zinczuk, J.; Brandán, S.A. Vibrational study of tolazoline hydrochloride by using FTIR-Raman and DFT calculations. *Spectrochim. Acta A* **2011**, *79*, 171**0-17**14, https://doi.org/10.1016/j.saa.2011.05.041.
17. Romano, E.; Brizuela, A.B.; Guzzetti, K.; Brandán, S.A. An experimental and theoretical study on the hydration in aqueous medium of the anti-hypertensive agent tolazoline hydrochloride. *J. Mol. Struct.* **2013**, *1037*, 393-401, http://dx.doi.org/10.1016/j.molstruc.2013.01.028.
18. Romano, E.; Davies, L.; Brandán, S.A. Structural properties and FTIR-Raman spectra of the anti-hypertensive, clonidine hydrochloride agent and their dimeric species. *J. Mol. Struct.* **2017**, *1133*, 226-235, http://dx.doi.org/10.1016/j.molstruc.2016.12.008.
19. Brandán, S.A. Correlations in hydrochloride drugs with diverse pharmacological activities. Role of N-H···Cl bonds. *Biointerface Research in Applied Chemistry* **2020**, *10*, 5536-5547, https://doi.org/10.33263/BRIAC103.536547.
20. http://www.emcdda.europa.eu/publications/drug-profiles/mdma
21. Clarke, E.G.C. *Isolation and Identification of Drugs.* 2nd Edition, The Pharmaceutical Press, 1986.
22. Galichat, L.Y. *Clarke's Analysis of Drugs and Poisons.* Pharmaceutical Press, Volume 2, 2004; pp. 1256.
23. Morimoto, B.H.; Lovell, S.; Karh, B. Organic Compounds Ecstasy: 3,4-Methylenedioxymethamphetamine (MDMA). *Acta Cryst.* **1998**, *C54*, 229-231.
24. Sondermann, N.; Kovar, K.A.. Identification of ecstasy in complex matrices using near-infrared spectroscopy. *Elsevier* **1999**, *102*, 133–147, https://doi.org/10.1016/S0379-0738(99)00047-X.
25. Sondermann, N.; Kovar. K-A. Screening experiments of ecstasy street samples using near infrared spectroscopy. *Elsevier* **1999**, *106*, 147–156, https://doi.org/10.1016/s0379-0738(99)00195-4.
26. Coates, J.; Reffner, J. Visualization of Micro-ATR Infrared Spectroscopy. *Spectroscopy* **1999**, *14*.
27. Lee, G.S.H.; Taylor, R.C.; Dawson, M.; Kannangara, G.S.K.; Wilson, M.A. High-resolution solid state 13C nuclear magnetic resonance spectra of 3,4-methylenedioxyamphetamine hydrochloride and related compounds and their mixtures with lactose. *Solid State Nuclear Magnetic Resonance* **2000**, *16*, 225-237, https://doi.org/10.1016/S0926-2040(00)00071-0.
28. Bell, S.E.J.; Burns, D.T.; Dennis, A.C.; Speers, J.S. Rapid analysis of ecstasy and related phenethylamines in seized tablets by Raman spectroscopy. *Analyst* **2000**, *125*, 541–544, https://doi.org/10.1039/a908091k.
29. Bell, S.E.J.; Burns, D.T.; Dennis A.C.; Matchett, L.J.; Speers, J.S.. Composition profiling of seized ecstasy tablets by Raman spectroscopy. *Analyst* **2000**, *125*, 1811–1815, https://doi.org/10.1039/b005662f.
30. Schneider, R.C.; Kovar, K.A. Analysis of ecstasy tablets: comparison of reflectance and transmittance near infrared spectroscopy. *Elsevier* **2003**, *134*, 187–195, https://doi.org/10.1016/s0379-0738(03)00125-7.
31. Zapata-Torres, G.; Cassels, B.K.; Parra-Mouchet, J.; Mascarenhas, Y.P.; Ellena, J.; De Araujo, A.S. Quantum-chemical, NMR and X-ray diffraction studies on ()-1-[3,4-(methylenedioxy)phenyl]-2-methylaminopropane. *Journal of Molecular Graphics & Modelling* **2008**, *26*, 1296-1305, https://doi.org/10.1016/j.jmgm.2007.12.004.
32. Müller, I.B.;Windberg, C.N.. Validation of an HPLC Method for Quantitation of MDMA in Tablets. *Journal of Chromatographic Science* **2005**, *43*, https://doi.org/10.1093/chromsci/43.8.434.
33. Milhazes, N.; Martins, P.; Uriarte E.; Garrido J.; Calheiros, R.; Marques, M.P.M.; Borges, F. Electrochemical and spectroscopic characterization of amphetamine-like drugs: Application to the screening of 3,4-methylenedioxymethamphetamine (MDMA) and its synthetic precursors. *Elsevier* **2007**, *596*, 231-241, https://doi.org/10.1016/j.aca.2007.06.027.
34. Allis, D.G.; Hakey, P.M.; Korter T.M. The solid terahertz spectrum of MDMA (Ecstacy) – A unique test for molecular modeling assignments. *Chemical Physics Letters* **2008**, *463*, 353-356, https://doi.org/10.1016/j.cplett.2008.08.024.

35. West, M.J.; Went M.J. The spectroscopic detection of drugs of abuse in fingerprints after development with powders and recovery with adhesive lifters. *Spectrochimica Acta Part A: Molecular and Biomolecular Spectroscopy* **2009**, *71*, 1984-198, https://doi.org/10.1016/j.saa.2008.07.024.
36. Hakey, P.M.; Allis, D.G.; Hudson, M.R.; Korter T.M. Density Functional Dependence in the Theoretical Analysis of the Terahertz Spectrum of the Illicit Drug MDMA (Ecstasy). *Ieee sensors journal* **2001**, *10.*
37. Liu, J.; Dacatur, J.; Proni, G.; Champeil E. Identification and quantitation of 3,4-methylenedioxy-N-methylamphetamphetamine (MDMA, ecstacy) in human urine by ^{1}H NMR spectroscopy. Application to five cases of intoxication. *Elsevier* **2010**, *194*, 103-107.
38. Ghafari, R.; Heydari, A.; Vardast, M.R.; Akbari A. HPLC Measurement of MDMA Content in Ecstasy Tablets Available in the Black Market of West Azerbaijan Province, Northwestern Iran. *Asia Pacific Journal of Medical Toxicology* **2014**.
39. Armenta, S.; Garrigues, S.; de la Guardia, M.; Brassier, J.; Alcalà, M.; Blanco, M. Analysis of ecstasy in oral fluid by ion mobility spectrometry and infrared spectroscopy after liquid–liquid extraction. *Journal of Chromatography A* **2015**, *1384*, 1-8, https://doi.org/10.1016/j.chroma.2015.01.036.
40. Barreiro, J.C.; Paixão, M.W.; Lourenço, T.C.; Cass, Q.B.; Venâncio, T. A High-Resolution Magic Angle Spinning NMR Study of the Enantiodiscrimination of 3,4-Methylenedioxymethamphetamine (MDMA) by an Immobilized Polysaccharide-Based Chiral Phase. *PLoS One* **2016**, *11*, https://doi.org/10.1371/journal.pone.0162892.
41. Almeida, NS.; Benedito, L.E.C.; Maldaner, A.O.; de Oliveira A.L.. A Validated NMR Approach for MDMA Quantification in Ecstasy Tablets. *J. Braz. Chem. Soc.* **2018**, *29*, 1944-1950, http://dx.doi.org/10.21577/0103-5053.20180071.
42. Zhong, Y.; Huang, K.; Luo, Q.; Yao, S.; Liu, X.; Yang, N.; Lin, C.; Luo, X. The Application of a Desktop NMR Spectrometer in Drug Analysis. *Int J Anal Chem* **2018**, *2018*, 3104569-3104569, https://doi.org/10.1155/2018/3104569.
43. Lourenço, T.C.; Bósio, G.C.; Cassiano, N.M.; Cass, Q.B.; Moreau, R.L.M. Chiral separation of 3,4-methylenedioxymethamphetamine (MDMA) enantiomers using batch chromatography with peak shaving recycling and its effects on oxidative stress status in rat liver. *Journal of Pharmaceutical and Biomedical Analysis* **2013**, *73*, 13-17, https://doi.org/10.1016/j.jpba.2012.01.025.
44. Becke, A.D. Density-functional exchange-energy approximation with correct asymptotic behavior. *Phys. Rev*. **1988**, *A38*, 3098-3100, https://doi.org/10.1103/PhysRevA.38.3098.
45. Lee, C.; Yang, W.; Parr. R.G. Development of the Colle-Salvetti correlation-energy formula into a functional of the electron density. *Phys. Rev*. **1988**, *B37*, 785-789, https://doi.org/10.1103/physrevb.37.785.
46. Miertus, S.; Scrocco, E.; Tomasi, J. Electrostatic interaction of a solute with a continuum. *Chem. Phys.* **1981,** *55*, 117–129, https://doi.org/10.1016/0301-0104(81)85090-2.
47. Tomasi, J.; Persico, J. Molecular Interactions in Solution: An Overview of Methods Based on Continous Distributions of the Solvent. *Chem. Rev*. **1994**, *94*, 2027-2094, https://doi.org/10.1021/cr00031a013.
48. Marenich, A.V.; Cramer, C.J.; Truhlar, D.G. Universal solvation model based on solute electron density and a continuum model of the solvent defined by the bulk dielectric constant and atomic surface tensions. *J. Phys. Chem.* **2009**, *B113*, 6378-6396, https://doi.org/10.1021/jp810292n.
49. Pulay P; Fogarasi G; Pongor G, Boggs JE; Vargha A. Combination of theoretical ab initio and experimental information to obtain reliable harmonic force constants. Scaled quantum mechanical (QM) force fields for glyoxal, acrolein, butadiene, formaldehyde, and ethylene. *J. Am. Chem. Soc*. **1983**, *105*, 7073-7047, https://doi.org/10.1021/ja00362a005
50. Rauhut, G.; Pulay, P. Transferable Scaling Factors for Density Functional Derived Vibrational Force Fields. *J. Phys. Chem*. **1995**, *99*, 3093-3100, https://doi.org/10.1021/j100010a019.
51. Sundius, T. Scaling of ab-initio force fields by MOLVIB. *Vib. Spectrosc*. **2002**, *29*, 89-95, https://doi.org/10.1016/S0924-2031(01)00189-8.
52. DL- 3,4- Methylenedioxymethamphetamine, Spectra BASE, https://spectrabase.com/spectrum/
53. Johnson, M.P.; Hoffman, A.J.; Nichols, D.E. Effects of the enantiomers of MDA, MDMA and related analogues on [3H] serotonin and [3H] dopamine release from superfused rat brain slices. *Eur. J. Pharmacol.* **1986**, *132*, 269-276, https://doi.org/10.1016/0014-2999(86)90615-1.
54. Schmidt, C.J.; Levin, J.A.; Loumberg, W. In vitro and in vivo neurochemical effects of methylenedioxymethamphetamine on striatal monoaminergic systems in the rat brain. *Biochem. Pharmacol*. **1987**, *36*, 747-755, https://doi.org/10.1016/0006-2952(87)90729-5.
55. Parr, R.G.; Pearson, R.G. Absolute hardness: companion parameter to absolute electronegativity. *J. Am. Chem. Soc.* **1983**, *105*, 7512-7516, https://doi.org/10.1021/ja00364a005.
56. Brédas, J.L. Mind the gap! *Materials Horizons* **2014**, *1*, 17–19, https://doi.org/10.1039/C3MH00098B.
57. Minteguiaga, M.; Dellacassa, E.; Iramain, M.A.; Catalán, C.A.N.; Brandán, S.A. Synthesis, spectroscopic characterization and structural study of 2-isopropenyl-3-methylphenol, carquejiphenol, a carquejol derivative with potential medicinal use. *J Mol. Struct*. **2018**, *1165*, 332-343, https://doi.org/10.1016/j.molstruc.2018.04.001.

58. M'leh, B.C.; Brandán, S.A.; Issaoui, N.; Roisnel, T.; Marouani, H. Synthesis, molecular structure, vibrational and theoretical studies of a new non-centrosymmetric organic sulphate with promising NLO properties. *J Mol. Struct.* **2018**, *1171*, 771-785, https://doi.org/10.1016/j.molstruc.2018.06.041.
59. Gatfaoui, S.; Issaoui, N.; Brandán, S.A.; Roisnel, T.; Marouani, H. Synthesis and characterization of p-xylylenediaminiumbis(nitrate). Effects of the coordination modes of nitrate groups on their structural and vibrational properties. *Journal of Molecular Structure* **2018**, *1151*, 152-168, http://dx.doi.org/10.1016/j.molstruc.2017.09.027.
60. Minteguiaga, M.; Dellacassa, E.; Iramain, M.A.; Catalán, C.A.N.; Brandán, S.A. FT-IR, FT-Raman, UV-Vis, NMR and structural studies of Carquejyl Acetate, a component of the essential oil from *Baccharis trimera* (Less.) DC. (Asteraceae). *J Mol. Struct*. **2019**, *1177*, 499-510, https://doi.org/10.1016/j.molstruc.2018.10.010.
61. Ruiz Hidalgo, J.; Neske, A.; Iramain, M.A.; Alvarez, P.E.; Leyton Bongiorno, P.; Brandán, S.A. FT-IR, FT-Raman and UV-visible spectra of motrilin acetogenin isolated from *Annona cherimolia. J Mol. Struct.* **2019**, *1196*, 508-517, https://doi.org/10.1016/j.molstruc.2019.06.107
62. Trabelsi, S.; Issaoui, N.; Brandán, S.A.; Bardak, F.; Roisnel, T.; Atac , A.; Marouani, H. Synthesis and physic-chemical properties of a novel chromate compound with potential biological applications, bis(2-phenylethylammonium) chromate(VI). *J Mol. Struct.* **2019**, *1185*, 168-182, https://doi.org/10.1016/j.molstruc.2019.02.106.
63. Iramain, M.A.; Castillo, M.V.; Davies, L.; María E. Manzur, M.E.; Brandán, S.A. Structural and SQMFF study of potent insecticide 40,40-DDT combining the FT-IR and FT-Raman spectra with DFT calculations. *J. Mol. Struct.* **2020**, *1199*, https://doi.org/10.1016/j.molstruc.2019.126964.
64. Kausteklis, J.; Aleksa, V.; Iramain, M.A.; Brandán, S.A. DFT study and vibrational assignment of 1-Butyl-3-methylimidazolium trifluoromethanesulfonate ionic liquid by using the FT-Raman spectrum. *J. Mol. Struct.* **2019**, *1175*, 663-676, https://doi.org/10.1016/j.molstruc.2018.08.014.
65. Iramain, M.A.; Davies, L.; Brandán, S.A. Structural and spectroscopic differences among the Potassium 5-hydroxypentanoyltrifluoroborate salt and the furoyl and isonicotinoyl salts. *J Mol. Struct*. **2019**, *1176*, 718-728, https://doi.org/10.1016/j.molstruc.2018.09.015.
66. A.B. Nielsen, A.J. Holder, Gauss View 3.0, User's Reference, GAUSSIAN Inc., Pittsburgh, PA, 2000–2003.
67. Frisch, M.J.; Trucks, G.W.; Schlegel, H.B.; Scuseria, G.E.; Robb, M.A.; Cheeseman, J.R.; Scalmani, G.; Barone, V.; Mennucci, B.; Petersson, G.A.; Nakatsuji, H.; Caricato, M.; Li, X.; Hratchian, H.P.; Izmaylov, A.F.; Bloino, J.; Zheng, G.; Sonnenberg, J.L.; Hada, M.; Ehara, M.; Toyota, K.; Fukuda, R.; Hasegawa, J.; Ishida, M.; Nakajima, T.; Honda, Y.; Kitao, O.; Nakai, H.; Vreven, T.; Montgomery, J.A.; Peralta, J.E.; Ogliaro, F.; Bearpark, M.; Heyd, J.J.; Brothers, E.; Kudin, K.N.; Staroverov, V.N.; Kobayashi, R.; Normand, J.; Raghavachari, K.; Rendell, A.; Burant, J.C.; Iyengar, S.S.; Tomasi, J.; Cossi, M.; Rega, N.; Millam, J.M.; Klene, M.; Knox, J.E.; Cross, J.B.; Bakken, V.; Adamo, C.; Jaramillo, J.; Gomperts, R.; Stratmann, R.E.; Yazyev, O.; Austin, A.J.; Cammi, R.; Pomelli, C.; Ochterski, J.W.; Martin, R.L.; Morokuma, K.; Zakrzewski, V.G.; Voth, G.A.; Salvador, P.; Dannenberg, J.J.; Dapprich, S.; Daniels, A.D.; Farkas, O.; Foresman, J.B.; Ortiz, J.; Cioslowski, J.; Fox, D.J. Gaussian, Inc., Wallingford CT, **2009**.
68. Ugliengo, P. Moldraw Program, University of Torino, Dipartimento Chimica IFM, Torino, Italy, 1998.
69. Glendening, E.; Badenhoop, J.K.; Reed, A.D.; Carpenter, J.E.; Weinhold, F. NBO 3.1; *Theoretical Chemistry Institute, University of Wisconsin; Madison*, WI, 1996.
70. Biegler-Köning, F.; Schönbohm, J.; Bayles, D. AIM2000; A Program to Analyze and Visualize Atoms in Molecules. *J. Comput. Chem.* **2001**, *22*, 545-559, https://doi.org/10.1002/1096-987X(20010415)22:5<545::AID-JCC1027>3.0.CO;2-Y.
71. Keresztury, G.; Holly, S.; Besenyei, G.; Varga, J. ;Wang, A.Y.; Durig, J.R. Vibrational spectra of monothiocarbamates-II. IR and Raman spectra, vibrational assignment, conformational analysis and ab initio calculations of **S**-methyl-**N,N**-dimethylthiocarbamate Spectrochim. Acta, **1993**, *49A*, 2007-2026.
72. Michalska, D.; Wysokinski, R. The prediction of Raman spectra of platinum(II) anticancer drugs by density functional theory. *Chemical Physics Letters* **2005**, *403*, 211-217.
73. Ditchfield, R. Self-consistent perturbation theory of diamagnetism. I. A gage invariant LCAO (linear combination of atomic orbitals) method for NMR chemical shifts. *Mol. Phys.* **1974**, *27*, 714-722.
74. R. Lazny, A. Ratkiewicz, A. Nodzewska, A. Wynimko, L. Siergiejczyk, Determination of the *N*-methyl stereochemistry in tropane and granatane derivatives in solution: a computational and NMR spectroscopic study. *Tetrahedron Letters* **2012.**
75. Besler, B.H.; Merz Jr, K.M.; Kollman, P.A. Atomic charges derived from demiempirical methods. *J. Comp. Chem.* **1990**, *11*, 431-439, https://doi.org/10.1002/jcc.540110404.
76. Bader, R.F.W. *Atoms in Molecules, A Quantum Theory.* Oxford University Press, Oxford, 1990.
77. Bushmarinov, I.S.; Lyssenko, K.A.; Antipin, M.Y. Atomic energy in the ′ Atoms in Molecules′ theory and its use for solving chemical problems. *Russian Chem. Rev*. **2009**, *78*, 283-302, https://doi.org/10.1070/RC2009v078n04ABEH004017.